The TOR signaling pathway regulates vegetative development, aflatoxin biosynthesis, and pathogenicity in *Aspergillus flavus*

Guoqi Li, Xiaohong Cao, Elisabeth Tumukunde, Qianhua Zeng, Shihua Wang*

Key Laboratory of Pathogenic Fungi and Mycotoxins of Fujian Province, Key Laboratory of Biopesticide and Chemical Biology of Education Ministry, and School of Life Sciences, Fujian Agriculture and Forestry University, Fuzhou, 350002, China.

Corresponding author:
Name: Shihua Wang Professor
School of Life Sciences,
Fujian Agriculture and Forestry University
Fuzhou, Fujian, 350002, China
Phone/Fax: +86-591-83789312
E-mail: wshyyl@sina.com

These authors contributed equally to this work.

Abstract

The target of rapamycin (TOR) signaling pathway is highly conserved and plays a crucial role in diverse biological processes in eukaryotes. However, the underlying mechanism of the TOR pathway in *A. flavus* remains elusive. In this study, we identified and characterized seven genes encoding various components of the TOR pathway in *A. flavus,* and investigated their biological function. The FK506-binding protein Fkbp3 and its lysine succinylation are important for aflatoxin production and rapamycin resistance. As a significant downstream effector molecule of the TorA kinase, the Sch9 kinase regulates aflatoxin B_1 (AFB_1) synthesis, osmotic and calcium stress response in *A. flavus,* and this regulation is mediated through its S_TKc, S_TK_X domains, and the ATP binding site at K340. We also showed that the Sch9 kinase may have a regulatory impact on the high-osmolarity glycerol (HOG) signaling pathway. TipA, the other downstream component of the TorA kinase, plays a significant role in regulating sclerotia formation and cell wall stress response in *A. flavus*. The members of the TapA-phosphatase complexes, SitA and Ppg1, are crucial for various biological processes in *A. flavus*, including vegetative growth, sclerotia formation, AFB_1 biosynthesis, and pathogenicity. Furthermore, we showed that SitA and Ppg1 are involved in regulating lipid droplets (LDs) biogenesis and cell wall integrity (CWI) signaling pathways. In addition, another phosphatase complex, Nem1/Spo7, plays critical roles in hyphal development, conidiation, aflatoxin, and lipid droplets biogenesis. This study provides an important insight into the regulatory

network of the TOR signaling pathway and the molecular mechanism of aflatoxin biosynthesis in *A. flavus*.

Keywords: *Aspergillus flavus*; the TOR signaling pathway; aflatoxin; vegetative development

Introduction

Aspergillus flavus is one of the most important phytopathogenic fungi that frequently contaminate various plants, causing economic losses in agricultural commodities and posing serious health concerns in developing countries [1]. *A. flavus* is also an opportunistic human pathogenic fungus that can cause aspergillosis in immune-compromised patients [2]. Aflatoxins (AFs), the toxic and carcinogenic secondary metabolites produced by *A. flavus*, are considered the most potent carcinogen present in nature, causing liver cancer in both humans and animals [3]. The aflatoxin biosynthesis is a complex process involving a series of reactions. Although the majority of the enzyme reactions and genes involved in aflatoxin biosynthesis have been elucidated [4], the related signaling pathway network and specific regulatory mechanisms governing aflatoxin biosynthesis remain elusive. Therefore, exploring the regulatory mechanism of the aflatoxin biosynthesis signaling pathway would provide new insights for preventing *A. flavus* and aflatoxin contamination.

In eukaryotes, the target of rapamycin (TOR) signaling pathway is highly conserved and plays essential roles in various significant biological processes, including ribosome biosynthesis, cell growth, and autophagy [5]. The

67 serine/threonine-protein kinase Tor serves as a crucial protein component in the TOR
68 signaling pathway, which interacts with other proteins to form multi-protein
69 complexes [6]. In *Saccharomyces cerevisiae*, TOR exists in two distinct multiprotein
70 functional complexes, namely TORC1 and TORC2 [7]. TORC1-mediated signaling
71 governs cellular growth by modulating various growth-related mechanisms and
72 exhibits sensitivity to rapamycin. Conversely, TORC2-mediated signaling primarily
73 regulates cytoskeletal remodeling but remains unaffected by rapamycin [7]. In yeast,
74 there are two *tor* genes, *tor1* and *tor2*, whereas in higher eukaryotes such as plants,
75 animals, and filamentous fungi, there is only one *tor* gene [8-10].

76 In the fungal kingdom, the TOR signaling pathway has been extensively
77 investigated in three prominent species: the budding yeast *S. cerevisiae* [11-12], the
78 fission yeast *Schizosaccharomyces pombe* [13-15], and the human pathogen *Candida*
79 *albicans* [16-17]. In *S. cerevisiae*, macrolide antibiotic rapamycin interacts with the
80 cytosolic protein Fkbp12 to form a complex, and the Fkbp12-rapamycin complex
81 effectively inhibits the activity of the Tor kinase function by binding to the FRB
82 domain [18]. The Tap42 phosphatase complex serves as the primary target of the Tor
83 kinase. Additionally, the Tap42 protein interacts with the Tip41 protein to
84 collaboratively regulate phosphatases, including PP2A and Sit4 [19-20]. Phosphatase
85 Sit4 can dephosphorylate the transcription factor Gln3, regulating the nitrogen source
86 metabolism pathway [21]. In addition, another immediate effector of TORC1 is the
87 AGC kinase Sch9, which participates in various cellular functions processes, such as
88 ribosome biosynthesis, translation initiation, and entry into the G_0 phase [22]. The TOR

89 signaling pathway has been documented in various filamentous fungi, including
90 *Fusarium graminearum* [23-24], *Magnaporthe oryzae* [25], *Phanerochaete*
91 *chrysosporium* [26], *Podospora anserine* [27], *A. nidulans* [28], *A. fumigatus* [29-30], *F.*
92 *fujikuroi* [31], *Botrytis cinerea* [32], *F. oxysporum* [33], and *Mucor circinelloides* [34].
93 However, the TOR signaling pathway has not yet been reported in *A. flavus*.

94 In eukaryotic cells, the TOR signaling pathway and the mitogen-activated protein
95 kinase (MAPK) signaling pathways play an important role in regulating adaptive
96 responses to extra- and intracellular conditions [35]. Several studies have demonstrated
97 that the TOR signaling pathway interacts with various other signaling pathways, such
98 as MAPK and cell wall integrity (CWI) pathway. These pathways engage in crosstalk,
99 forming a complex metabolic network that regulates cellular processes [36-40]. However,
100 the underlying mechanisms of multiple crosstalks between the TOR and other
101 signaling pathways in *A. flavus* remain unclear. Therefore, we intended to identify the
102 genes associated with the TOR signaling pathway and elucidate their roles and
103 contributions in regulating vegetative development and aflatoxin biosynthesis in *A.*
104 *flavus*. Our results demonstrated that the TOR signaling pathway is involved in
105 multiple cellular processes in *A. flavus*. Our findings revealed a complex interplay
106 between the TOR pathway and other signaling pathways (such as HOG and CWI) in
107 *A. flavus*, which play a crucial role in regulating cellular growth and survival under
108 environmental stress conditions.

109 # Results

110 **Rapamycin exhibits inhibitory effects on the growth, sporulation, sclerotia**
111 **formation, and aflatoxin production in *A. flavus***

112 Rapamycin, a secondary metabolite synthesized by *Streptomyces hygroscopicus*,
113 exhibits efficacy in suppressing specific filamentous fungi. In *F. graminearum*,
114 rapamycin has a significant inhibitory impact on growth and asexual reproduction [23].
115 To investigate the effects of rapamycin on vegetative development, sclerotia
116 formation, and secondary metabolism in *A. flavus*, we conducted an assay to
117 determine the sensitivity of the wild-type strain to rapamycin. We observed that the
118 wild-type strain exhibited a high sensitivity to rapamycin. We found that 100 ng/mL
119 of rapamycin significantly inhibited mycelial growth and conidia formation (Fig. 1A,
120 1D, 1E). More importantly, the wild-type strain exhibited a significant reduction in
121 sclerotia formation and aflatoxin synthesis (Fig. 1B, 1C, 1F, 1G). Additionally,
122 rapamycin resulted in a significant decrease in spore germination rate and sparser
123 conidiophores (Fig. S1A, S1B). These results illustrated that the TOR signaling
124 pathway may be involved in regulating the growth, development, and secondary
125 metabolism of *A. flavus.* Calcofluor white is a chemifluorescent blue dye commonly
126 employed for its nonspecific binding affinity to fungal chitin. Fluorescence
127 microscopy analysis revealed a notable reduction in the blue fluorescence on the cell
128 wall following treatment with rapamycin (Fig. S1C). The intracellular lipid droplets
129 within the hyphae were labeled with BODIPY. We observed that the hyphae treated

130 with rapamycin contained more lipid droplets compared to the control group (Fig.
131 S1D). These findings suggest that the TOR pathway may play important roles in
132 maintaining cell wall integrity and facilitating the biogenesis of lipid droplets.

133 To investigate the potential regulatory role of the TOR pathway in modulating
134 the sporulation, sclerotia formation, and aflatoxin biosynthesis in *A. flavus*, we
135 examined the expression levels of conidia-related, sclerotia formation-related, and
136 aflatoxin-related genes after 3, 6, and 9 hours of treatment with rapamycin. To
137 determine the effects of rapamycin on conidiation, qRT-PCR was conducted to assess
138 the transcript levels of two conidia-related genes, *abaA* and *brlA*. We also conducted
139 qRT-PCR to evaluate the expression levels of three regulators (*nsdC*, *nsdD*, and *sclR*)
140 involved in sclerotia development, and genes involved in AFB_1 biosynthesis, such as
141 the regulatory gene *aflS*, as well as several structural genes (*aflC* and *aflQ*). The
142 strains treated with rapamycin exhibited a significant reduction in the expression
143 levels of genes related to sporulation, sclerotia formation, and aflatoxin synthesis (Fig.
144 1H, 1I, 1J). Overall, these results indicated that the TOR pathway plays a crucial role
145 in regulating the growth, sporulation, sclerotia formation, and aflatoxin biosynthesis
146 in *A. flavu*s by modulating the expression of these genes.

147 **The impact of Fkbp3 and its lysine succinylation on AFB_1 biosynthesis and**
148 **rapamycin resistance in *A. flavus***

149 FK506-binding proteins (Fkbps) belong to a highly conserved immunophilin
150 family, which are involved in various cellular functions, such as protein folding,
151 immunosuppression, signaling transduction, and transcription [41]. Fkbps function as

152 molecular switches by binding to target proteins and inducing conformational changes
153 [41]. In *S. cerevisiae*, Fkbp12 and rapamycin interact to form a complex that exerts a
154 negative regulatory effect on the activity of the Tor kinase [42]. The *fkbp12* gene
155 homologue *fprA* in *A. nidulans* shares high levels of homology with that from *S.*
156 *cerevisiae* [28]. According to the protein sequence of FprA from *A. nidulans*, four genes
157 encoding putative proteins with FK506 binding domain, named *fkbp1*
158 (AFLA_126880), *fkbp2* (AFLA_087480), *fkbp3* (AFLA_010910), and *fkbp4*
159 (AFLA_128200), have been identified from the *A. flavus* genome. We generated four
160 *fkbp* knockout strains using homologous recombination, and all *fkbp* disruption strains
161 were confirmed by PCR and sequencing analysis (Fig. S2). Phenotypic analyses
162 showed that the mycelial growth and conidia formation of all the *fkbp* mutants were
163 similar to the wild-type strain on the PDA medium (Fig. 2A), suggesting that Fkbps
164 have minimal influence on the process of vegetative development. We evaluated AFB_1
165 synthesis utilizing thin layer chromatography (TLC), and the findings demonstrated a
166 noteworthy reduction in AFB_1 synthesis upon deletion of Fkbp3, in comparison to the
167 wild-type strain (Fig. 2B, 2D). Additionally, the quantity of sclerotia exhibited a
168 significant decrease in all *fkbp* mutants compared to the wild-type strain (Fig. S3A,
169 S3B). The aforementioned data indicated that Fkbp3 plays a crucial role in sclerotia
170 formation and aflatoxin biosynthesis in *A. flavus*.

171 To determine the specific Fkbp responsible for rapamycin sensitivity, all mutant
172 strains were cultured on PDA solid plates amended with 100 ng/mL rapamycin. The
173 strain with disrupted *fkbp3* showed significant resistance to rapamycin, while the

174 deletion mutants of *fkbp1*, *fkbp2*, and *fkbp4* did not exhibit any alteration in resistance
175 to rapamycin (Fig. 2A, 2C). These results demonstrated that Fkbp3 serves as the
176 principal target for rapamycin in *A. flavu*s. In the FK506-sensitivity analysis, we
177 observed a significant suppression of mycelial growth and conidia formation in
178 wild-type strain with the addition of 10 ng/mL FK506 to the PDA medium.
179 Additionally, the deletion of *fkbp3* led to the heightened resistance to FK506
180 compared to the wild-type strain (Fig. 2A, 2C). These findings suggested that Fkbp3
181 is mainly involved in the modulation of FK506 resistance in *A. flavus*.

182 Previous studies have shown that lysine succinylation plays a significant role in
183 aflatoxin production and pathogenicity in *A. flavus* [43]. Based on the analysis of our
184 succinylome data, we have identified six reliable succinylation sites (K5, K19, K40,
185 K42, K55, and K65) on the Fkbp3 protein. To identify the function of Fkbp3
186 succinylation sites, site-directed mutations were constructed according to the
187 homologous recombination strategy. Compared to the wild-type strain, all point
188 mutants exhibited a similar phenotype in vegetative growth and conidiation.
189 Interestingly, we observed that the K19A mutation resulted in increased resistance to
190 rapamycin (Fig. 2E, 2F). Additionally, the K19A strain exhibited a significant
191 reduction in the production of AFB_1 compared to the wild-type strain (Fig. 2G, 2H).
192 These findings suggested that the succinylation of Fkbp3 at K19 plays a crucial role in
193 rapamycin resistance and aflatoxin biosynthesis. Furthermore, we found that various
194 point mutants, including K40A, K42A, and K55A, exhibited reduced levels of AFB_1
195 production in comparison to the wild-type strain (Fig. 2G, 2H), suggesting that the

196 succinylation of Fkbp3 at other sites also contributes to AFB_1 biosynthesis in *A. flavus*.
197 The above results indicated that the K19 site likely plays a more prominent role in
198 Fkbp3 succinylation compared to other sites.

199 **The Sch9 kinase is involved in aflatoxin biosynthesis and the HOG pathway**

200 Sch9, a Ser/Thr kinase belonging to the AGC family, is directly phosphorylated by
201 TORC1. The phosphorylation of Sch9 is inhibited by rapamycin, as well as by carbon
202 or nitrogen starvation [22]. The putative *sch9* gene (AFLA_127440) in *A. flavus*
203 encodes a protein consisting of 706 amino acids, exhibiting 80.31% identity to the
204 Sch9 protein in *A. nidulans*. To investigate the role of Sch9 in *A. flavus*, we attempted
205 to create a *sch9* deletion mutant using a homologous recombination strategy. The
206 Δ*sch9* strain exhibited typical vegetative growth and conidiation similar to the
207 wild-type strain (Fig. 3B). TLC assay and quantitative analysis showed a significantly
208 decreased aflatoxin production in the Δ*sch9* strain compared to the wild-type strain
209 (Fig. 3C, 3G). These results indicated that Sch9 regulates aflatoxin biosynthesis in *A.*
210 *flavus*.

211 In yeast, Sch9 plays an important role in the transcriptional activation of
212 osmostress inducible genes [44]. To characterize the roles of Sch9 in stress response,
213 we examined the sensitivity of the *sch9* deletion strain to various stresses including
214 osmotic stress and calcium stress. Compared with the wild-type strain, the Δ*sch9*
215 mutant significantly increased sensitivity to calcium stress (Fig. S4A, S4B), and
216 decreased sensitivity to osmotic stress induced by NaCl and KCl (Fig. 3D, 3H). In *A.*
217 *flavus*, the Sch9 kinase consists of several domains, including the protein kinase C

218 conserved region 2 (C2), protein kinase (S_TKc), AGC-kinase C-terminal (S_TK_X)
219 domain, and an ATP binding site (Fig. 3A). To explore the role of these domains and
220 the ATP binding site in Sch9 kinase, we constructed deletion strains for both domains
221 and a *sch9*^{K340A} mutant. The results revealed that the *sch9*$^{\Delta S_TKc}$ strain, *sch9*$^{\Delta S_TK_X}$
222 strain, and *sch9*^{K340A} mutant exhibited similar phenotypes in osmotic stress and AFB_1
223 production as the Δ*sch9* mutant (Fig. 3B, 3C, 3D). Therefore, we speculate that the
224 protein kinase domain, kinase C-terminal domain, and the ATP binding site at K340
225 play a crucial role in modulating the impact of Sch9 on aflatoxin biosynthesis and
226 stress response in *A. flavus*.

227 To investigate the potential function of Sch9 in the HOG and TOR pathways in *A.*
228 *flavus*, we conducted a sensitivity analysis of the Δ*sch9* strain to rapamycin.
229 Compared to the wild-type strain, the *sch9* deletion strain exhibited a slightly higher
230 sensitivity to rapamycin (Fig. 3B, 3F). The MAKP Hog1 is an element of the high
231 osmolarity glycerol (HOG) pathway. To verify the connection between Sch9 and the
232 HOG-MAPK pathway, the phosphorylation levels of Hog1 kinase were measured
233 under osmotic stress (1M NaCl). Western blot analysis showed that the
234 phosphorylation level of Hog1 increased significantly in the Δ*sch9* strain (Fig. 3E).
235 This finding suggested that Sch9 plays a pivotal role in modulating the response of
236 Hog1 to osmotic stress. Taken together, these results reflected that Sch9 regulates
237 osmotic stress response via the HOG pathway in *A. flavus*.

238 **TipA participate in regulation of sclerotia development and cell wall stress**
239 **response**

240 In *S. cerevisiae*, Tip41 was identified as a Tap42-interacting protein and has been
241 measured to function as a negative regulator of Tap42, which downregulates TORC1
242 signaling via activation of PP2A phosphatase [45]. The putative orthologue of *tip41* in
243 *A. flavus* is named *tipA* (AFLA_047310). The amino acid sequence of TipA exhibits a
244 similarity of 40.49% to Tip41 in *S. cerevisiae*. To elucidate the function of the TOR
245 signaling pathway protein TipA in *A. flavus*, we generated the *tipA* deletion mutants.
246 The Δ*tipA* strain exhibited a slightly reduced number of conidia produced on PDA
247 compared to the wild-type strain (Fig. 4A, 4C). Meanwhile, the Δ*tipA* strain exhibited
248 decreased sensitivity to rapamycin (Fig. 4A, 4E). The Δ*tipA* strain was unable to
249 produce any sclerotia (Fig. 4B, 4F). Whereas Δ*tipA* strain do not affect aflatoxin
250 production(Fig. 4D, 4G). In addition, the Δ*tipA* strain was more sensitive to the cell
251 wall and cell membrane stress, including CR and SDS (Fig. 4H, 4I). Additionally, the
252 expression levels of *nsdC* and *nsdD* exhibited a decrease in Δ*tipA* strain compared to
253 the wild-type strain (Fig. 4J). These results indicated that TipA is crucial for the
254 sclerotial formation and cell wall stress in *A. flavus*.

255 **Phosphatase SitA and Ppg1 are involved in growth, conidiation, and sclerotial**
256 **formation**

257 In *S. cerevisiae*, Tap42 has been identified to interact with the catalytic subunit of
258 type 2A protein phosphatases, including Pph3, Pph21, and Pph22, as well as the type
259 2A-like phosphatases Sit4 and Ppg1[19]. Phosphatase *sitA* (AFLA_108450) and *ppg1*
260 (AFLA_132610) were identified in *A. flavu*s, encoding putative orthologs of *sit4* and
261 *ppg1* in *S. cerevisiae.* To determine the biological functions of phosphatase SitA and

262 Ppg1 in *A. flavus*, we disrupted the *sitA* and *ppg1* by homologous recombination
263 strategy. To further investigate the relationship between phosphatase SitA and Ppg1,
264 we additionally generated complemented and double deletion mutants. The vegetative
265 development phenotype analysis showed that the Δ*sitA*, Δ*ppg1*, and Δ*sitA*/Δ*ppg1*
266 strains grew significantly more slowly than the wild-type strain on PDA (Fig. 5A, 5D).
267 Additionally, the Δ*sitA*, Δ*ppg1*, and Δ*sitA*/Δ*ppg1* strains were more sensitive to
268 rapamycin (Fig. 5A, 5E). In addition, the Δ*sitA*, Δ*ppg1*, and Δ*sitA*/Δ*ppg1* strains
269 formed lower number of conidiophores (Fig. 5A). To gain further insight into the role
270 of SitA and Ppg1 in the process of conidiation, qRT-PCR was employed to determine
271 the transcript levels of conidiation-related genes (*abaA* and *brlA*). The expression
272 levels of the *abaA and brlA* genes were significantly downregulated in the Δ*sitA*,
273 Δ*ppg1*, and Δ*sitA*/Δ*ppg1* mutants when compared to the wild-type and complemented
274 strains (Fig. 5G). The analysis of sclerotial formation revealed that the Δ*sitA*, Δ*ppg1*,
275 and Δ*sitA*/Δ*ppg1* mutants exhibited a complete inability to produce any sclerotia (Fig.
276 5B, 5E). To further prove these findings, we conducted qRT-PCR to determine the
277 expression levels of three regulators (*nsdC*, *nsdD*, and *sclR*) of sclerotia development.
278 Our findings indicated that the expression levels of *nsdC*, *nsdD*, and *sclR* were all
279 significantly reduced in the Δ*sitA*, Δ*ppg1*, and Δ*sitA*/Δ*ppg1* mutants (Fig. 5H), which
280 is consistent with the observed decrease in sclerotia production in the Δ*sitA*, Δ*ppg1*,
281 and Δ*sitA*/Δ*ppg1* mutants. These results showed that SitA and Ppg1 are crucial for
282 hyphal development, conidiation, and sclerotia formation in *A. flavus*.

283 **SitA and Ppg1 play crucial roles in aflatoxin biosynthesis and pathogenicity**

284 We assayed AFB_1 biosynthesis in the Δ*sitA*, Δ*ppg1*, and Δ*sitA*/Δ*ppg1* mutants.
285 TLC analyses revealed that the Δ*sitA* and Δ*sitA*/Δ*ppg1* strains exhibited a decrease in
286 AFB_1 production, whereas the Δ*ppg1* strain showed a significant increase in AFB_1
287 production compared to the wild-type and complemented strains (Fig. 5C, 5F). The
288 expression levels of genes related to aflatoxin synthesis, including structural genes
289 (*aflO* and *aflP*) and regulatory genes (*aflR* and *aflS*), were determined by qRT-PCR in
290 the Δ*sitA*, Δ*ppg1*, and Δ*sitA*/Δ*ppg1* mutants. The results revealed a significant
291 downregulation of these genes in the Δ*sitA* and Δ*sitA*/Δ*ppg1* mutants, while
292 upregulated in the Δ*ppg1* mutants, compared to the wild-type and complemented
293 strains (Fig. 5I). These results indicated that SitA and Ppg1 play different roles in
294 regulating aflatoxin biosynthesis in *A. flavu*s.
295 We conducted pathogenicity tests on peanuts and maize to examine the
296 pathogenicity of the phosphatases SitA and Ppg1 on crops. The results showed that
297 the wild-type and complemented strains demonstrated complete virulence on all
298 peanut and maize seeds. In contrast, the Δ*sitA*, Δ*ppg1*, and Δ*sitA*/Δ*ppg1* mutants
299 displayed compromised colonization on peanut and maize seeds (Fig. 6A). In addition,
300 the number of conidial productions in these mutants on the infected peanut seeds also
301 dramatically decreased compared to those of the wild-type and complemented strains
302 (Fig. 6C). The thin-layer chromatography analyses revealed that the Δ*ppg1* mutant
303 exhibited increased production of AFB_1 in peanuts and maize. Conversely, the levels
304 of aflatoxin produced by the Δ*sitA* and Δ*sitA*/Δ*ppg1* mutants on peanut and maize
305 were significantly reduced compared to the wild-type and complemented strains (Fig.

306 6B, 6D). This observation aligns with the above results of aflatoxin biosynthesis from
307 all mutant strains in the YES medium. All these data showed that SitA and Ppg1 are
308 crucial for crop seeds' pathogenicity.

309 **SitA and Ppg1 are involved in regulating cell wall integrity**

310 To explore the role of phosphatases SitA and Ppg1 in response to cell wall stress,
311 all strains were cultivated on PDA amended with CFW, CR, and SDS. We found that
312 the relative growth inhibition of Δ*sitA*, Δ*ppg1*, and Δ*sitA*/Δ*ppg1* mutants induced by
313 cell wall stress was significantly increased compared to the wild-type and
314 complemented strains (Fig. 7A, 7B). Further investigations using qRT-PCR revealed a
315 notable reduction in the expression levels of genes related to the synthesis of cell
316 walls, specifically chitin synthase genes *chsA*, *chsD*, and *chsE* in the Δ*sitA*, Δ*ppg1*,
317 and Δ*sitA*/Δ*ppg1* strains (Fig. 7C). Western blot analysis also revealed that the
318 phosphorylation level of Slt2 was significantly elevated in the Δ*sitA*, Δ*ppg1*, and
319 Δ*sitA*/Δ*ppg1* strains under cell wall stress (200 μg/ml CFW) (Fig. 7D). In conclusion,
320 the phosphatases SitA and Ppg1 play a crucial role in regulating cell wall integrity.

321 **The phosphatase complex Nem1/Spo7 is important for growth, aflatoxin**
322 **biosynthesis, and LD biogenesis**

323 Lipid droplets (LDs) are highly dynamic spherical organelles, which appear in
324 the cytosol of most eukaryotic cell types[46]. Rapamycin treatment led to the
325 accumulation of lipid droplets in various filamentous fungi [24]. The FgTOR pathway
326 regulates the phosphorylation status of FgNem1 mainly via the
327 FgPpg1/Sit4-FgCak1/other kinase cascade in *F. graminearum* [24]. In this study, we

328 observed that the treatment of hyphae with rapamycin resulted in the accumulation of
329 LD biogenesis (Fig. 8A). This finding suggested that the TOR pathway may regulate
330 the LD biogenesis. However, the underlying regulatory mechanism of LD
331 biosynthesis remain largely unknown in *A. flavu*s. To investigate the regulatory
332 mechanism of the TOR pathway in *A. flavus* that controls LD biogenesis, we
333 examined LD accumulation in Δ*sch9*, Δ*sitA*, and Δ*ppg1* mutants. BODIPY staining
334 assays revealed that LD biogenesis was not observed in the Δ*sitA* and Δ*ppg1* strains
335 upon treatment with rapamycin, in contrast to the wild-type and Δ*sch9* strains (Fig.
336 8A, 8B, 8C, 8D). These results indicated that LD biogenesis induced by rapamycin is
337 predominantly reliant on the phosphatases SitA and Ppg1 in *A. flavus*. In *F.*
338 *graminearum*, the phosphatase FgNem1/FgSpo7 complex was involved in the
339 induction of LD biogenesis by rapamycin[24]. Phosphatase *nem1* (AFLA_002649) and
340 *spo7* (AFLA_028590) were identified in *A. flavu*s, which encode putative orthologs of
341 *nem1* and *spo7* in *F. graminearum.* To examine the role of the *nem1* and *spo7* genes in
342 *A. flavus*, we generated Δ*nem1* and Δ*spo7* mutants using homologous recombination.
343 The Δ*nem1* and Δ*spo7* mutants displayed a notable reduction in both vegetative
344 growth and conidiation compared to the wild-type strain (Fig. 9A, 9C, 9D). TLC
345 assay revealed a significantly decreased aflatoxin production in the Δ*nem1* and Δ*spo7*
346 compared to the wild-type strain (Fig. 9B). In addition, BODIPY staining showed no
347 visible lipid droplets in the hyphae of Δ*nem1* and Δ*spo7* after rapamycin treatment
348 (Fig. 9E). Taken together, these results indicated that Nem1/Spo7 are involved in
349 vegetative growth, conidiation, aflatoxin production, and LD biogenesis.

350 # Discussion

351 Aflatoxins (AFs) are a class of toxic secondary metabolites synthesized by *A.*
352 *flavus*, including aflatoxin B_1, B_2, G_1, and G_2, among which AFB_1 has been regarded
353 as the most pathogenic and toxic aflatoxin[47]. Therefore, understanding the regulatory
354 mechanisms involved in fungal secondary metabolites biosynthesis would be
355 instrumental for effectively addressing aflatoxin control in *A. flavus*. In this study, we
356 demonstrated that the target of rapamycin (TOR) signaling pathway plays a pivotal
357 role in regulating growth, sporulation, sclerotia formation, aflatoxin production, and
358 various stress responses in *A. flavus*. Through conducting functional studies on genes
359 within the TOR signaling pathway, we explored the conservation and complexity
360 exhibited by the TOR signaling pathway in *A. flavu*s. In addition, we constructed a
361 crosstalk network between the TOR and other signaling pathways (HOG, CWI) and
362 analyzed the specific regulatory process. We proposed that the TOR signaling
363 pathway interacts with multiple signaling pathways, including HOG and CWI
364 pathways, to modulate the cellular responses to diverse environmental stresses (Fig.
365 10).

366 We have observed that rapamycin has a significant impact on the growth and
367 sporulation of *A. flavus* (Fig. 1A). Additionally, it exhibits a strong inhibitory effect on
368 sclerotia production and aflatoxin biosynthesis (Fig. 1B, 1C). The inhibitory effect has
369 been documented in various fungal species, including *Candida albicans* [48],
370 *Cryptococcus neoformans* [48], *Podospora anserine* [27], *A. nidulans* [28], *Magnaporthe*

371 *oryzae* [39], and *F. graminearum* [23]. This suggested that the TOR signaling pathway
372 may have a conserved function in filamentous fungi. The number of FK506-binding
373 proteins varies among different species: there are four Fkbps proteins in *S. cerevisiae*
374 and three Fkbps proteins in *S. pombe* [49]. In *S. cerevisiae*, rapamycin can bind to Fkbp
375 protein, resulting in the irreversible inhibition of the G_1 phase of the cell cycle and the
376 regulation of cell growth [50]. In *A. nidulans,* the *fkbp12* gene homologue *fprA* displays
377 considerable sequence similarity with homologues identified in the *S. cerevisiae* [28].
378 In this study, based on the homologous alignment of the protein sequence of FprA, it
379 was observed that four *fkbp* genes are present in *A. flavus*. Among these, deletion of
380 *fkbp3* exhibited enhanced tolerance to rapamycin (Fig. 2A). So we speculated that
381 rapamycin forms a complex with Fkbp3 in *A. flavus*, subsequently targeting
382 downstream target genes to exert its biological function. We found that Fkbp3 is
383 involved in sclerotia formation and aflatoxin biosynthesis in *A. flavus* (Fig. 2A, S3),
384 and subsequent analysis revealed that the underlying mechanism may be associated
385 with succinylation modification. The succinylation sites of Fkbp3 were identified
386 through the utilization of succinylation proteomics data. By constructing point mutant
387 strains and conducting phenotype experiments, we found that the succinylation of
388 Fkbp3 at residue K19 is involved in rapamycin resistance and aflatoxin biosynthesis
389 (Fig. 2E, 2G). Previous studies have demonstrated that Fkbp12 has been identified as
390 the receptor for FK506 and rapamycin, which inhibits calcineurin and target
391 rapamycin complex 1 (TORC1), respectively [50]. The deletion of Fkbp12 confers the
392 resistance to rapamycin in *C. albicans* [48] and *C. neoformans* [48]. The

393 entomopathogenic fungus *Beauveria bassiana* contains three putative *fkbp* genes, and
394 disruption of *Bbfkbp12* significantly increases the resistance to rapamycin and FK506
395 [51]. The plant pathogenic fungus *F. graminearum* harbors three Fkbps proteins, among
396 which deletion of *Fgfkbp12* leads to resistance to rapamycin [23]. Thus, we propose
397 that these Fkbps may exhibit analogous functionalities in conferring resistance to
398 rapamycin. In *Botrytis cinerea*, deletion of *Bcfkbp12* caused a reduction of the
399 virulence of strain T4, while knockout of the *fkbp12* gene did not affect the
400 pathogenic development of strain B05.10 [32]. These findings demonstrated that the
401 *fkbp12* homologous genes exhibited conservation in terms of rapamycin resistance.
402 However, there is significant variation in other biological functions among fungal
403 species, which may be attributed to species or strain evolutionary divergence.

404 The Tor kinase functions as a fundamental component of the TOR signaling
405 pathway, which exhibits evolutionary conservation across fungi, plants, and mammals
406 [52]. In *S. cerevisiae*, the Tor kinase can interact with a diverse range of proteins,
407 resulting in the formation of complex structures known as TORC1 and TORC2 [53].
408 TORC1 can detect various signals, including nutrients, growth factors, and
409 environmental stress. It plays a crucial role in regulating cellular processes such as
410 gene transcription, protein translation, ribosome synthesis, and autophagy [54]. A
411 characteristic that distinguishes TORC1 is its interaction with KOG1 (Raptor in
412 mammals) and its sensitivity to the rapamycin-FKBP12 complex [55]. Almost all other
413 eukaryotes, including plants, worms, flies, and mammals, have a single *tor* gene,
414 whereas *S. cerevisiae* has two *tor* genes [54]. The Tor kinase is widely conserved both

415 in terms of its structural characteristics and its role as the target of Fkbp-rapamycin.
416 Typically, the Tor kinase exhibits similar structural characteristics, including the
417 HEAT-like, FAT, FRB, kinase, and FATC domains. The FRB domain is the binding
418 region of the Fkbp-rapamycin complex, and rapamycin resistance is usually caused by
419 the disruption of the FRB domain [54]. The comparison of homology and the analysis
420 of phylogenetics revealed that there is only one predicted *torA* gene in *A. flavus*. To
421 ascertain its functionality, several ectopic transformants were obtained through
422 multiple protoplast transformations, however, no successful knock-out transformants
423 were obtained. We speculated that the deletion of the *torA* gene may be lethal in *A.*
424 *flavus*. This observation aligns with the situation observed in *F. graminearum* [23].
425 Previous findings demonstrated that the Tor kinase could function as a molecular
426 switch connecting an iron cue to defend against pathogen infection in *C. elegans* [56].
427 In *A. fumigatus*, the Tor kinase represents a central regulatory node controlling genes
428 and proteins involved in nutrient sensing, stress response, cell cycle progression,
429 protein biosynthesis, and degradation, as well as adaptation to low iron conditions[57].
430 In summary, the Tor kinase acts as a central regulator in the TOR signaling pathway,
431 playing a crucial role in the regulation of the cell cycle, protein synthesis, and cellular
432 energy metabolism.

433 In *S. cerevisiae*, the protein kinase Sch9 is a major downstream effector of
434 TORC1, and this kinase is known to have crucial functions in stress resistance,
435 longevity, and nutrient sensing [44]. In addition, the TORC1-Sch9 pathway acts as a
436 crucial mediator of chronological lifespan [44]. In filamentous fungi, an intricate

437 network of interactions exists between the TOR and HOG pathways. In *F.*
438 *graminearum* [38], FgSch9 and FgHog1 mutants displayed heightened susceptibility to
439 osmotic and oxidative stresses. The phosphorylation level of FgHog1 increased
440 significantly in FgSch9 mutant. Additionally, the affinity capture-MS assay showed
441 that the Tor kinase was among the proteins co-purifying with FgSch9. These results
442 suggest that FgSch9 serves as an intermediary for the TOR and HOG signaling
443 pathways [38]. Furthermore, FgSch9 plays a crucial role in the regulation of various
444 biological processes such as hyphal differentiation, asexual development, virulence,
445 and DON biosynthesis[38]. In *A. fumigatus*, the SchA mutant was sensitive to
446 rapamycin, high concentrations of calcium and hyperosmotic stress, and SchA was
447 involved in iron metabolism. The SchA mutant exhibited enhanced phosphorylation
448 of SakA in response to osmotic stress [29]. In this study, we discovered that Sch9 is
449 involved in regulating aflatoxin biosynthesis (Fig. 3C), and responses to osmotic
450 stress and rapamycin stress (Fig. 3B, 3D). The S_TKc domain deletion strain
451 ($sch9^{\Delta S_TKc}$), S_TK_X domain deletion strain ($sch9^{\Delta S_TK_X}$), and $sch9^{K340A}$ mutant
452 displayed a similar phenotype to the Δ*sch9* strain (Fig. 3B, 3C, 3D). These findings
453 revealed that Sch9 plays a significant role in the biological synthesis of aflatoxin and
454 in responding to various stresses. This role is primarily mediated through its kinase
455 domain, kinase-C domain, and ATP binding site K340. We also found that the
456 phosphorylation level of Hog1 increased significantly in the Δ*sch9* strain under
457 osmotic stress (Fig. 3E). Based on the above results, we hypothesized that Sch9 was
458 involved in the osmotic stress response by modulating the HOG pathway.

459 Tap42, a protein that associates with phosphatase 2A, serves as the direct target
460 of the Tor kinase in yeast. Tap42 plays a crucial role in various Tor functions,
461 particularly in the regulation of transcriptional processes [58]. The genome of *A. flavus*
462 contains a homolog of *tap42* named *tapA* (AFLA_092770), which is predicted to
463 encode a 355 amino-acid protein (sharing 31.9% identity with *S. cerevisiae* Tap42).
464 To further determine the function of the TapA regulator in the TOR signaling pathway
465 of *A. flavus*, we conducted targeted gene deletion experiments on *tapA*. We failed to
466 obtain a null mutant, we hypothesised that *tapA* knockout was lethal in *A. flavus*. In *S.*
467 *pombe*, the protein Tip41, which interacts with Tap42, plays a significant role in the
468 cellular responses to nitrogen sources by regulating type 2A phosphatases [59]. In *S.*
469 *cerevisiae*, Tap42-phosphatase complexes associate with TORC1, whereas Tip41
470 functions to attenuate TORC1 signaling by stimulating the PP2A phosphatase [45].
471 Unlike its yeast counterpart Tip41, TIPRL, a mammalian Tip41-like protein, exerts a
472 positive influence on mTORC1 signaling by interacting with PP2Ac [60]. While the
473 interaction between Tip41 and Tap42 was not observed in the filamentous fungi. The
474 yeast two-hybrid (Y2H) assay showed that FgTip41 interacts with the phosphatase
475 FgPpg1 rather than FgTap42, while the FgTap42 bind with phosphatases FgPp2A,
476 implying that FgTap42, FgPpg1, and FgTip41 form a heterotrimer in *F. graminearum*
477 [23]. In the rice blast fungus *M. oryzae*, MoTip41 does not interact with MoTap42.
478 However, MoTip41 can bind with the phosphatase MoPpe1, thereby facilitating
479 crosstalk between the TOR pathway and the cell wall integrity pathway [40]. In this
480 study, we found that TipA played a crucial role in sclerotia production and cell wall

481 stress in *A. flavus* (Fig. 4B, 4H). However, the interaction between TapA and TipA is
482 not yet clear in *A. flavus*.

483 In *S. cerevisiae*, Tap42 can bind and regulate various PP2A phosphatases,
484 including Pph3, Pph21, Pph22, Sit4, and Ppg1. This interaction plays a crucial role in
485 the TOR signaling pathway, particularly in response to rapamycin treatment or
486 nutrient deprivation [45]. The phosphatase Sit4 plays a crucial role in regulating cell
487 growth, morphogenesis, and virulence in *C. albicans* [61]. FgSit4 and FgPpg1 are
488 associated with various cellular processes, including mycelial growth, conidiation,
489 DON biosynthesis, and virulence in *F. graminearum* [23]. In addition, FgSit4 and
490 FgPpg1 are involved in the regulation of various signaling pathways, such as the CWI
491 pathway and lipid droplets biogenesis regulation pathway [23]. In this study, we found
492 that the phosphatase SitA and Ppg1 play critical role in vegetative growth, conidiation,
493 sclerotia formation, and aflatoxin biosynthesis in *A. flavus* (Fig. 5A, 5B, 5C).
494 Additionally, the phosphatase SitA and Ppg1 also affect pathogenicity and LD
495 biogenesis (Fig. 6A, 8C, 8D). In addition, SitA, Ppg1, and TipA exhibits similar
496 functions in sclerotia production and cell wall stress response. Based on these
497 observations, we hypothesized that TapA-phosphatase complexes play a collaborative
498 role in the regulation of the sclerotia formation and cell wall stress response in *A.*
499 *flavus.*

500 After the deletion of the *sitA* and *ppg1* genes, the expression level of genes
501 related to cell wall synthesis has decreased significantly, resulting in damage to the
502 cell wall and showing a higher sensitivity to cell wall integrity stress (Fig. 7C).

503 Western blotting results showed that the phosphorylation level of MAPK kinase Slt2
504 has increased significantly in the Δ*sitA* and Δ*ppg1* strains under cell wall stress,
505 indicating that SitA and Ppg1 exert a negative regulatory effect on the CWI pathway
506 (Fig. 7D). In *M. oryzae*, MoPpe1 and MoSap1 serve as an adaptor complex that
507 connects the CWI and TOR signaling pathways. Activation of the TOR pathway
508 results in the inhibition of the CWI pathway [39]. In addition, the phosphatase MoPpe1
509 interacts with the phosphatase-associated protein MoTip41, facilitating the exchange
510 of information between the TOR and CWI signaling pathways [39]. These results
511 suggest that the phosphatase Ppe1 engages in interactions with various proteins to
512 effectively coordinate the TOR and CWI signaling pathways, thereby regulating the
513 growth and pathogenicity of the rice blast fungus *M. oryzae* [39]. Taken together, we
514 speculated that the phosphatase SitA and Ppg1 might exhibit differential regulation in
515 the CWI and TOR pathways across species in order to fulfill their respective
516 functions.

517 In *F. graminearum,* the phosphatase complex FgNem1/Spo7-FgPah1 cascade
518 plays significant roles in fungal development, DON production, and lipid droplet (LD)
519 biogenesis [24]. In this study, our results indicated that Nem1 and Spo7 are important
520 for vegetative growth and secondary metabolism of *A. flavus* (Fig. 9A, 9B). We have
521 also discovered that LD biogenesis is facilitated by the Nem1/Spo7 and SitA/Ppg1
522 pathways (Fig. 8C, 8D, 9E). These observations suggest that the PP2A phosphatases
523 play a central role as core phosphatases in the LD biogenesis signaling network.
524 However, there are likely other kinases involved in the regulation of LD biogenesis.

525 To gain a comprehensive understanding of the precise molecular mechanism, further
526 research should focus on investigating the interplay between phosphatases and other
527 kinases.

528 In conclusion, we identified the complex regulatory network that provides insight
529 into the interplay between the TOR, HOG, and CWI signaling pathways, and how
530 they collectively regulate the development, aflatoxin biosynthesis, and pathogenicity
531 of *A. flavus*. By elucidating the functions of genes associated with the TOR signaling
532 pathway, our research could establish a solid foundation for comprehending the
533 molecular mechanism underlying the aflatoxin biosynthesis of *A. flavus*. This, in turn,
534 can provide novel insights into the management of aflatoxin contamination and the
535 mitigation of *A. flavus* infection.

536 Materials and methods

537 Strains and cultural conditions

538 The *A. flavus* strains in this study were shown in Table S1. All strains were
539 cultivated on three different types of agar media: potato dextrose agar (PDA), yeast
540 extract-sucrose agar (YES), and yeast extract-glucose agar (YGT). The growth and
541 conidiation assays were conducted at 37℃. Additionally, aflatoxin production was
542 assessed using YES liquid medium at 29℃.

543 Constructions of gene deletion and complemented mutants

544 The construction of gene deletion and complemented strains was carried out
545 using the SOE-PCR strategy, following previously established protocols [62]. The

546 primers utilized for the amplification of the flanking sequences of each gene can be
547 found in Table S2. The putative gene deletion mutants were validated through PCR
548 assays using the appropriate primers (Fig. S2), and their confirmation was
549 subsequently obtained through sequencing analysis.

550 **Growth, conidiation, and sclerotia analysis**

551 To evaluate mycelial growth and conidia formation, 1 μL of 10^6 spores/mL conidia
552 of all strains was point inoculated onto the center of the PDA medium, and then
553 cultured at 37°C for 5 days in the dark. The conidia were washed with 0.07%
554 Tween-20 and counted using a hemocytometer and microscope [43]. For sclerotia
555 formation analysis, each strain was inoculated and cultivated on CM agar medium at
556 37°C in the dark for 7 days, and then 75% ethanol was used to wash away mycelia
557 and conidia on the surface of the medium [63]. These assays were repeated at least
558 three times.

559 **Extraction and quantitative analysis of aflatoxin**

560 To extract and quantify aflatoxins (AFs) production, 1 μL of 10^6 spores/mL
561 conidia of all strains was point inoculated onto liquid YES medium, and cultures were
562 then incubated at 29°C in the dark for 6 days. AFs were extracted from the media and
563 detected using thin layer chromatography (TLC) [63]. In addition, the standard AFB_1
564 was employed for visual comparison, and AFs were quantitatively analyzed using the
565 Image J tool. The assays were repeated at least three times.

566 **Stress assay**

567 To determine the roles of the gene in *A. flavus* responsing to various
568 environmental stresses, 1 μL of 10^6 spores/mL conidia of all strains were point
569 inoculated onto these PDA solid plates supplemented with various agents. These
570 agents included 1M NaCl, 1M KCl, and 1M $CaCl_2$ for inducing osmotic stress, as
571 well as 100 μg/mL SDS, 200 μg/mL Calcofluor white (CFW), and 200 μg/mL Congo
572 red (CR) for inducing cell wall stress. After 5 days of incubation at 37°C in the dark,
573 the relative rates of inhibition were determined [43]. The assays were repeated at least
574 three times.

575 **Seeds infection assays**

576 To measure the pathogenicity of *A. flavus*, all peanut and maize seeds were
577 washed in 0.05% sodium hypochlorite, 75% ethanol, and sterile water, respectively.
578 Subsequently, all peanut and maize seeds were immersed in sterile water containing
579 10^6 spores/mL of all strains at 29°C in the dark for 60 min. After the conidia adhesion,
580 the seeds were cultured at 29°C for 6 days in the dark [64].

581 **Quantitative RT-PCR**

582 For the real-time quantitative PCR (qPCR) assays, the *A. flavus* strains were
583 cultivated in the PDA medium at 29°C for 3 days in the dark. Total RNA was
584 extracted from the mycelia of all strains, and cDNA was synthesized with the First
585 Strand cDNA Synthesis Kit, and then the cDNA was used as the template for
586 qRT-PCR analysis with SYBR Green qPCR mix. The relative transcript level of each
587 gene was calculated by the $2^{-\Delta\Delta CT}$method [65].

588 **Western blot analysis**

589 To extract the total protein, the mycelia of each strain were cultivated in YES
590 liquid medium for 48 h, then the sample was grinded under liquid nitrogen to a fine
591 powder and transferred to a 1.5 mL microcentrifuge tube added with RIPA lysis buffer
592 and 1 mM PMSF protease inhibitor. Proteins were separated by 12% SDS-PAGE and
593 transferred onto a polyvinylidene fluoride (PVDF) membrane. Phosphorylation levels
594 of Hog1 and Slt2 were detected by Phospho-p38 MAPK antibody (Cell Signaling
595 Technology, Boston, MA, USA) and Phospho-p44/42 MAPK (Erk 1/2) antibody (Cell
596 signaling Technology, MA, USA), respectively. The experiment was conducted three
597 times independently.

598 **Statistical analysis**

599 All data were measured with means ± standard deviation (SD) of three biological
600 replicates. Graph Pad Prism 7 software was used for conducting statistical and
601 significance analysis, and p-values < 0.05 represented statistical significance.
602 Student's *t*-test was used to compare the two means for differences, whereas Tukey's
603 multiple comparisons were used for testing multiple comparisons.

604 # Acknowledgments

605 The authors also thank Professor Zhenhong Zhuang, Jun Yuan, Yu Wang, Kunzhi
606 Jia, Xiuna Wang, and Xinyi Nie for their help in the experiments. This work was
607 supported by the National Natural Science Foundation of China (Grant No.
608 31972214).

609 # Author contributions

610 Guoqi Li and Xiaohong Cao designed the experiments. Guoqi Li, Xiaohong Cao,
611 and Qianhua Zeng performed the experiments. Guoqi Li, Xiaohong Cao, and Shihua
612 Wang analyzed the data. Guoqi Li, Elisabeth Tumukunde, and Shihua Wang wrote the
613 manuscript. The manuscript was discussed and revised by all the authors.

614 **References**

615 [1] Klich MA. *Aspergillus flavus*: the major producer of aflatoxin. Mol Plant Pathol.
616 2007; 8(6): 713-22.
617 [2] Hedayati MT, Pasqualotto AC, Warn PA, et al. *Aspergillus flavus*: human
618 pathogen, allergen and mycotoxin producer. Microbiology (Reading). 2007;
619 153(Pt 6): 1677-1692.
620 [3] Khan R, Ghazali FM, Mahyudin NA, et al. Biocontrol of aflatoxins using
621 non-aflatoxigenic *Aspergillus flavus*: a literature review. J Fungi (Basel). 2021;
622 7(5): 381.
623 [4] Yabe K, Nakajima H. Enzyme reactions and genes in aflatoxin biosynthesis. Appl
624 Microbiol Biotechnol. 2004; 64(6): 745-55.
625 [5] Wullschleger S, Loewith R, Hall MN. TOR signaling in growth and metabolism.
626 Cell. 2006; 124(3): 471-84.
627 [6] De Virgilio C, Loewith R. The TOR signalling network from yeast to man. Int J
628 Biochem Cell Biol. 2006; 38(9): 1476-1481.
629 [7] Loewith R, Jacinto E, Wullschleger S, et al. Two TOR complexes, only one of
630 which is rapamycin sensitive, have distinct roles in cell growth control. Mol Cell.

631 2002; 10(3): 457-68.

632 [8] Beauchamp EM, Platanias LC. The evolution of the TOR pathway and its role in
633 cancer. Oncogene. 2013 Aug 22; 32(34): 3923-32.

634 [9] Fu L, Liu Y, Qin G, et al. The TOR-EIN2 axis mediates nuclear signalling to
635 modulate plant growth. Nature. 2021; 591(7849): 288-292.

636 [10] Teichert S, Wottawa M, Schönig B, et al. Role of the *Fusarium fujikuroi* TOR
637 kinase in nitrogen regulation and secondary metabolism. Eukaryot Cell. 2006;
638 5(10): 1807-1819.

639 [11] Crespo JL, Hall MN. Elucidating TOR signaling and rapamycin action: lessons
640 from *Saccharomyces cerevisiae*. Microbiol Mol Biol Rev. 2002; 66(4): 579-591.

641 [12] Rohde JR, Bastidas R, Puria R, et al. Nutritional control via Tor signaling in
642 *Saccharomyces cerevisiae*. Curr Opin Microbiol. 2008; 11(2): 153-60.

643 [13] Ishiguro J, Shibahara K, Ueda Y, et al. Fission yeast TOR signaling is essential
644 for the down-regulation of a hyperactivated stress-response MAP kinase under
645 salt stress. Mol Genet Genomics. 2013; 288(1-2): 63-75.

646 [14] Otsubo Y, Yamamato M. TOR signaling in fission yeast. Crit Rev Biochem Mol
647 Biol. 2008; 43(4): 277-83.

648 [15] Petersen J. TOR signalling regulates mitotic commitment through stress-activated
649 MAPK and Polo kinase in response to nutrient stress. Biochem Soc Trans. 2009;
650 37(Pt1): 273-7.

651 [16] Bastidas RJ, Heitman J, Cardenas ME. The protein kinase Tor1 regulates adhesin
652 gene expression in *Candida albicans*. PLoS Pathog. 2009; 5(2): e1000294.

653 [17] Liu NN, Flanagan PR, Zeng J, et al. Phosphate is the third nutrient monitored by
654 TOR in *Candida albicans* and provides a target for fungal-specific indirect TOR
655 inhibition. Proc Natl Acad Sci U S A. 2017; 114(24): 6346-6351.
656 [18] Hu K, Guo S, Yan G, et al. Ubiquitin regulates TORC1 in yeast *Saccharomyces*
657 *cerevisiae*. Mol Microbiol. 2016; 100(2): 303-314.
658 [19] Wang H, Wang X, Jiang Y. Interaction with Tap42 is required for the essential
659 function of Sit4 and type 2A phosphatases. Mol Biol Cell. 2003; 14(11): 4342-51.
660 [20] Yan G, Shen X, Jiang Y. Rapamycin activates Tap42-associated phosphatases by
661 abrogating their association with Tor complex 1. EMBO J. 2006; 25(15):
662 3546-55.
663 [21] Tate JJ, Tolley EA, Cooper TG. Sit4 and PP2A dephosphorylate nitrogen
664 catabolite repression-sensitive Gln3 when TorC1 is up- as well as downregulated.
665 Genetics. 2019; 212(4): 1205-1225.
666 [22] Urban J, Soulard A, Huber A, et al. Sch9 is a major target of TORC1 in
667 *Saccharomyces cerevisiae*. Mol Cell. 2007; 26(5): 663-74.
668 [23] Yu F, Gu Q, Yun Y, et al. The TOR signaling pathway regulates vegetative
669 development and virulence in *Fusarium graminearum*. New Phytol. 2014; 203(1):
670 219-32.
671 [24] Liu N, Yun Y, Yin Y, et al. Lipid droplet biogenesis regulated by the
672 FgNem1/Spo7-FgPah1 phosphatase cascade plays critical roles in fungal
673 development and virulence in *Fusarium graminearum*. New Phytol. 2019; 223(1):
674 412-429.

675 [25] Sun G, Elowsky C, Li G, et al. TOR-autophagy branch signaling via Imp1
676 dictates plant-microbe biotrophic interface longevity. PLoS Genet. 2018; 14(11):
677 e1007814.
678 [26] Nguyen DV, Roret T, Fernandez-Gonzalez A, et al. Target of rapamycin pathway
679 in the white-rot fungus *Phanerochaete chrysosporium*. PLoS One. 2020; 15(2):
680 e0224776.
681 [27] Dementhon K, Paoletti M, Pinan-Lucarré B, et al. Rapamycin mimics the
682 incompatibility reaction in the fungus *Podospora anserina*. Eukaryot Cell. 2003;
683 2(2): 238-46.
684 [28] Fitzgibbon GJ, Morozov IY, Jones MG, et al. Genetic analysis of the TOR
685 pathway in *Aspergillus nidulans*. Eukaryot Cell. 2005; 4(9): 1595-8.
686 [29] Alves de Castro P, Dos Reis TF, et al. The *Aspergillus fumigatus* SchA^{SCH9} kinase
687 modulates SakA^{HOG1} MAP kinase activity and it is essential for virulence. Mol
688 Microbiol. 2016; 102(4): 642-671.
689 [30] Baldin C, Valiante V, Krüger T, et al. Comparative proteomics of a tor inducible
690 *Aspergillus fumigatus* mutant reveals involvement of the Tor kinase in iron
691 regulation. Proteomics. 2015; 15(13): 2230-43.
692 [31] Teichert S, Wottawa M, Schönig B, et al. Role of the *Fusarium fujikuroi* TOR
693 kinase in nitrogen regulation and secondary metabolism. Eukaryot Cell. 2006;
694 5(10): 1807-19.
695 [32] Meléndez HG, Billon-Grand G, Fèvre M, et al. Role of the *Botrytis cinerea*
696 FKBP12 ortholog in pathogenic development and in sulfur regulation. Fungal

697 Genet Biol. 2009; 46(4): 308-20.

698 [33] López-Berges MS, Rispail N, Prados-Rosales RC, et al. A nitrogen response
699 pathway regulates virulence functions in *Fusarium oxysporum* via the protein
700 kinase TOR and the bZIP protein MeaB. Plant Cell. 2010; 22(7): 2459-75.

701 [34] Bastidas RJ, Shertz CA, Lee SC, et al. Rapamycin exerts antifungal activity *in*
702 *vitro* and *in vivo* against *Mucor circinelloides* via FKBP12-dependent inhibition
703 of Tor. Eukaryot Cell. 2012; 11(3): 270-81.

704 [35] Madrid, M, Vázquez-Marín, B, Franco, A, et al. Multiple crosstalk between TOR
705 and the cell integrity MAPK signaling pathway in fission yeast. Sci Rep. 2016
706 Nov 23; 6: 37515.

707 [36] Torres J, Di Como CJ, Herrero E, et al. Regulation of the cell integrity pathway
708 by rapamycin-sensitive TOR function in budding yeast. J Biol Chem. 2002 Nov 8;
709 277(45): 43495-504.

710 [37] Chen DD, Shi L, Yue SN, et al. The Slt2-MAPK pathway is involved in the
711 mechanism by which target of rapamycin regulates cell wall components in
712 *Ganoderma lucidum*. Fungal Genet Biol. 2019; 123: 70-77.

713 [38] Gu Q, Zhang C, Yu F, et al. Protein kinase FgSch9 serves as a mediator of the
714 target of rapamycin and high osmolarity glycerol pathways and regulates multiple
715 stress responses and secondary metabolism in *Fusarium graminearum*. Environ
716 Microbiol. 2015; 17(8): 2661-76.

717 [39] Qian B, Liu X, Jia J, et al. MoPpe1 partners with MoSap1 to mediate TOR and
718 cell wall integrity signalling in growth and pathogenicity of the rice blast fungus

719 *Magnaporthe oryzae*. Environ Microbiol. 2018; 20(11): 3964-3979.

720 [40] Qian B, Liu X, Ye Z, et al. Phosphatase-associated protein MoTip41 interacts
721 with the phosphatase MoPpe1 to mediate crosstalk between TOR and cell wall
722 integrity signalling during infection by the rice blast fungus *Magnaporthe oryzae*.
723 Environ Microbiol. 2021; 23(2): 791-809.

724 [41] Tong M, Jiang Y. FK506-binding proteins and their diverse functions. Curr Mol
725 Pharmacol. 2015; 9(1): 48-65.

726 [42] Heitman J, Movva NR, Hall MN. Targets for cell cycle arrest by the
727 immunosuppressant rapamycin in yeast. Science. 1991; 253(5022): 905-9.

728 [43] Ren S, Yang M, Yue Y, et al. Lysine succinylation contributes to aflatoxin
729 production and pathogenicity in *Aspergillus flavus*. Mol Cell Proteomics. 2018;
730 17(3): 457-471.

731 [44] Pascual-Ahuir A, Proft M. The Sch9 kinase is a chromatin-associated
732 transcriptional activator of osmostress-responsive genes. EMBO J. 2007; 26(13):
733 3098-108.

734 [45] Jacinto E, Guo B, Arndt KT, et al. TIP41 interacts with TAP42 and negatively
735 regulates the TOR signaling pathway. Mol Cell. 2001; 8(5): 1017-26.

736 [46] Sánchez-Álvarez M, Del Pozo MÁ, Bosch M, et al. Insights into the biogenesis
737 and emerging functions of lipid droplets from unbiased molecular profiling
738 approaches. Front Cell Dev Biol. 2022 Jun 8; 10: 901321.

739 [47] Gizachew D, Chang CH, Szonyi B, et al. Aflatoxin B1 (AFB_1) production by
740 *Aspergillus flavus* and *Aspergillus parasiticus* on ground Nyjer seeds: The effect

741 of water activity and temperature. Int J Food Microbiol. 2019; 296: 8-13.

742 [48] Cruz MC, Goldstein AL, Blankenship J, et al. Rapamycin and less
743 immunosuppressive analogs are toxic to *Candida albicans* and *Cryptococcus*
744 *neoformans* via FKBP12-dependent inhibition of TOR. Antimicrob Agents
745 Chemother. 2001; 45(11): 3162-70.

746 [49] Galat A. Functional diversity and pharmacological profiles of the FKBPs and
747 their complexes with small natural ligands. Cell Mol Life Sci. 2013; 70(18):
748 3243-75.

749 [50] Kasahara K. Physiological function of FKBP12, a primary target of
750 rapamycin/FK506: a newly identified role in transcription of ribosomal protein
751 genes in yeast. Curr Genet. 2021 Jun; 67(3): 383-388.

752 [51] Li Y, Ren H, Zhao Y, et al. Characterization of three FK506-binding proteins in
753 the entomopathogenic fungus *Beauveria bassiana*. J Invertebr Pathol. 2020; 171:
754 107334.

755 [52] Xiong Y, Sheen J. The role of target of rapamycin signaling networks in plant
756 growth and metabolism. Plant Physiol. 2014; 164(2): 499-512.

757 [53] Weisman R. Target of rapamycin (TOR) regulates growth in response to
758 nutritional signals. Microbiol Spectr. 2016 Oct; 4(5).

759 [54] Loewith R, Hall MN. Target of rapamycin (TOR) in nutrient signaling and
760 growth control. Genetics. 2011 Dec; 189(4): 1177-201.

761 [55] Adami A, García-Alvarez B, Arias-Palomo E, et al. Structure of TOR and its
762 complex with KOG1. Mol Cell. 2007; 27(3): 509-16.

763 [56] Ma YC, Dai LL, Qiu BB, et al. TOR functions as a molecular switch connecting
764 an iron cue with host innate defense against bacterial infection. PLoS Genet. 2021;
765 17(3): e1009383.
766 [57] Baldin C, Valiante V, Krüger T, et al. Comparative proteomics of a tor inducible
767 *Aspergillus fumigatus* mutant reveals involvement of the Tor kinase in iron
768 regulation. Proteomics. 2015; 15(13): 2230-43.
769 [58] Düvel K, Broach JR. The role of phosphatases in TOR signaling in yeast. Curr
770 Top Microbiol Immunol. 2004; 279: 19-38.
771 [59] Fenyvuesvolgyi C, Elder RT, Benko Z, et al. Fission yeast homologue of
772 Tip41-like proteins regulates type 2A phosphatases and responses to nitrogen
773 sources. Biochim Biophys Acta. 2005; 1746(2): 155-62.
774 [60] Nakashima A, Tanimura-Ito K, Oshiro N, et al. A positive role of mammalian
775 Tip41-like protein, TIPRL, in the amino-acid dependent mTORC1-signaling
776 pathway through interaction with PP2A. FEBS Lett. 2013; 587(18): 2924-9.
777 [61] Han Q, Pan C, Wang Y, et al. PP2A-like protein phosphatase (Sit4) regulatory
778 subunits, Sap155 and Sap190, regulate *Candida albicans*' cell growth,
779 morphogenesis, and virulence. Front Microbiol. 2019 Dec 20; 10: 2943.
780 [62] Tan L, Chen H, Yu S, et al. A SOE-PCR method of introducing multiple
781 mutations into Mycoplasma gallisepticum neuraminidase. J Microbiol Methods.
782 2013; 94(2): 117-120.
783 [63] Nie X, Yu S, Qiu M, et al. *Aspergillus flavus* SUMO contributes to fungal
784 virulence and toxin attributes. J Agric Food Chem. 2016 Sep 7; 64(35): 6772-82.

785 [64] Wang Y, Wang S, Nie X, et al. Molecular and structural basis of nucleoside
786 diphosphate kinase-mediated regulation of spore and sclerotia development in the
787 fungus *Aspergillus flavus*. J Biol Chem. 2019 Aug 16; 294(33): 12415-12431.
788 [65] Livak KJ, Schmittgen TD. Analysis of relative gene expression data using
789 real-time quantitative PCR and the $2^{-\Delta\Delta CT}$ method. Methods. 2001; 25(4):
790 402–408.
791 [66] Chang PK, Scharfenstein LL, Wei Q, Bhatnagar D. Development and refinement
792 of a high-efficiency gene-targeting system for Aspergillus flavus. J Microbiol
793 Methods. 2010 Jun;81(3):240-6.

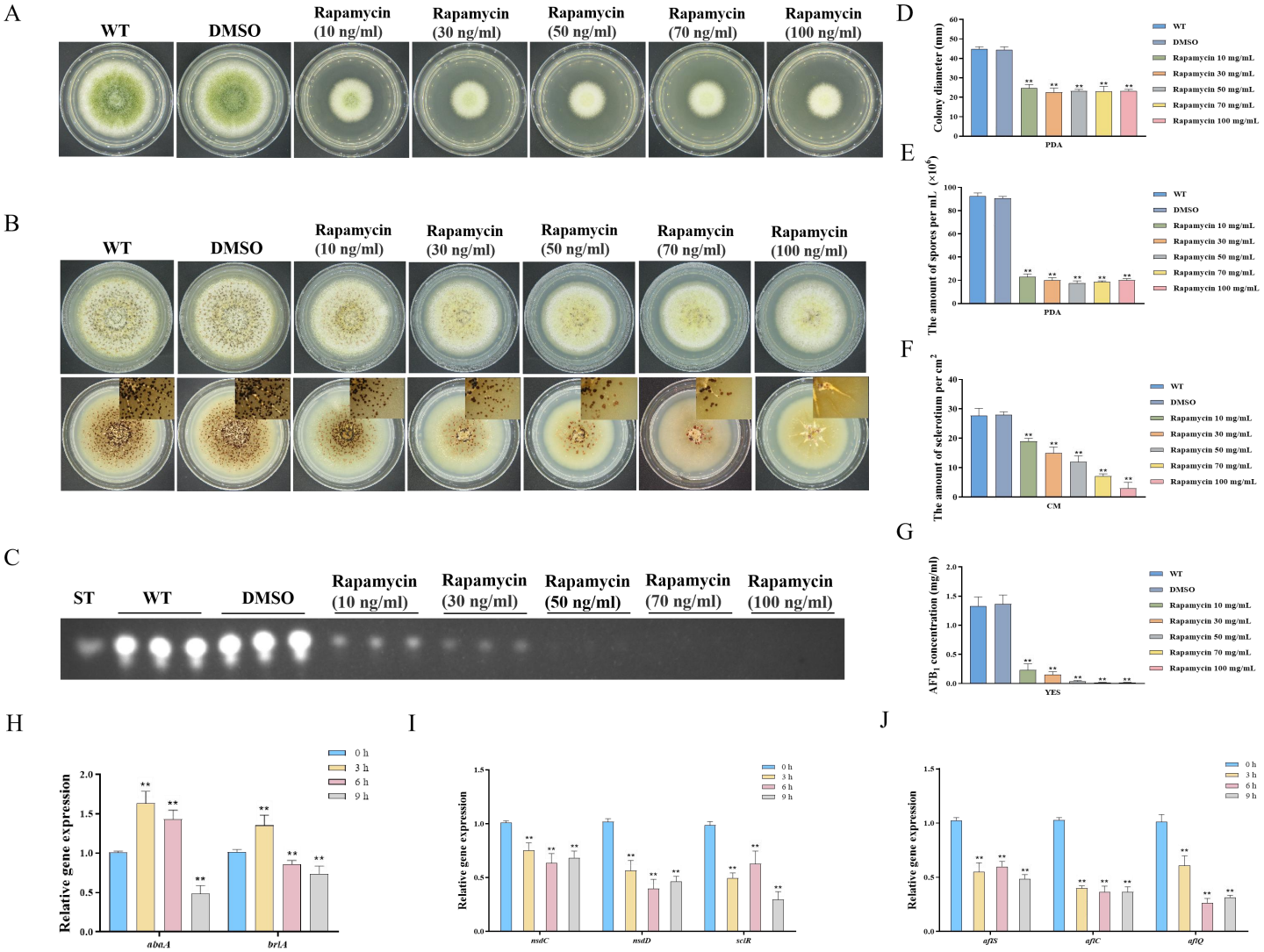
A
WT
DMSO
Rapamycin (10 ng/ml)
Rapamycin (30 ng/ml)
Rapamycin (50 ng/ml)
Rapamycin (70 ng/ml)
Rapamycin (100 ng/ml)
B
C
ST
D
Colony diameter (mm)
PDA
E
The amount of spores per mL (×10^6)
F
The amount of sclerotium per cm^2
CM
G
AFB1 concentration (mg/ml)
YES
Rapamycin 10 mg/mL
Rapamycin 30 mg/mL
Rapamycin 50 mg/mL
Rapamycin 70 mg/mL
Rapamycin 100 mg/mL
H
Relative gene expression
0 h
3 h
6 h
9 h
abaA
brlA
I
nsdC
nsdD
sclR
J
aflS
aflC
aflQ

Fig. 1 Impacts of rapamycin on the growth, sporulation, sclerotia formation,and aflatoxin production of *Aspergillus flavus*.

(A) Colony morphology of the WT strain cultured on PDA medium amended with different concentrations of rapamycin at 37°C for 5 days.

(B) Colony phenotype of the WT strain grown on CM medium amended with different concentrations of rapamycin at 37°C for 7 days.

(C) TLC assay of AFB_1 production by the WT strain cultured in YES liquid media amended with different concentrations of rapamycin at 29°C for 6 days.

(D) Statistical analysis of the colony diameter by the WT strain treated with different concentrations of rapamycin described in (A).

(E) Conidial quantification of the WT strain treated with different concentrations of rapamycin as mentioned in (A).

(F) Quantitative analysis of sclerotium formation by the WT strain treated with different concentrations of rapamycin described in (B).

(G) Relative quantification of AFB_1 production by the WT strain treated with different concentrations of rapamycin as mentioned in (C)

(H) Relative expression levels of conidia-related genes in WT strain treated with 100 ng/mL rapamycin after 3, 6, 9 h.

(I) Relative expression levels of sclerotia-related genes in WT strain treated with 100 ng/mL rapamycin after 3, 6, 9 h.

(J) Relative expression levels of aflatoxin biosynthesis regulatory and structural genes in WT strain treated with 100 ng/mL rapamycin after 3, 6, 9 h.

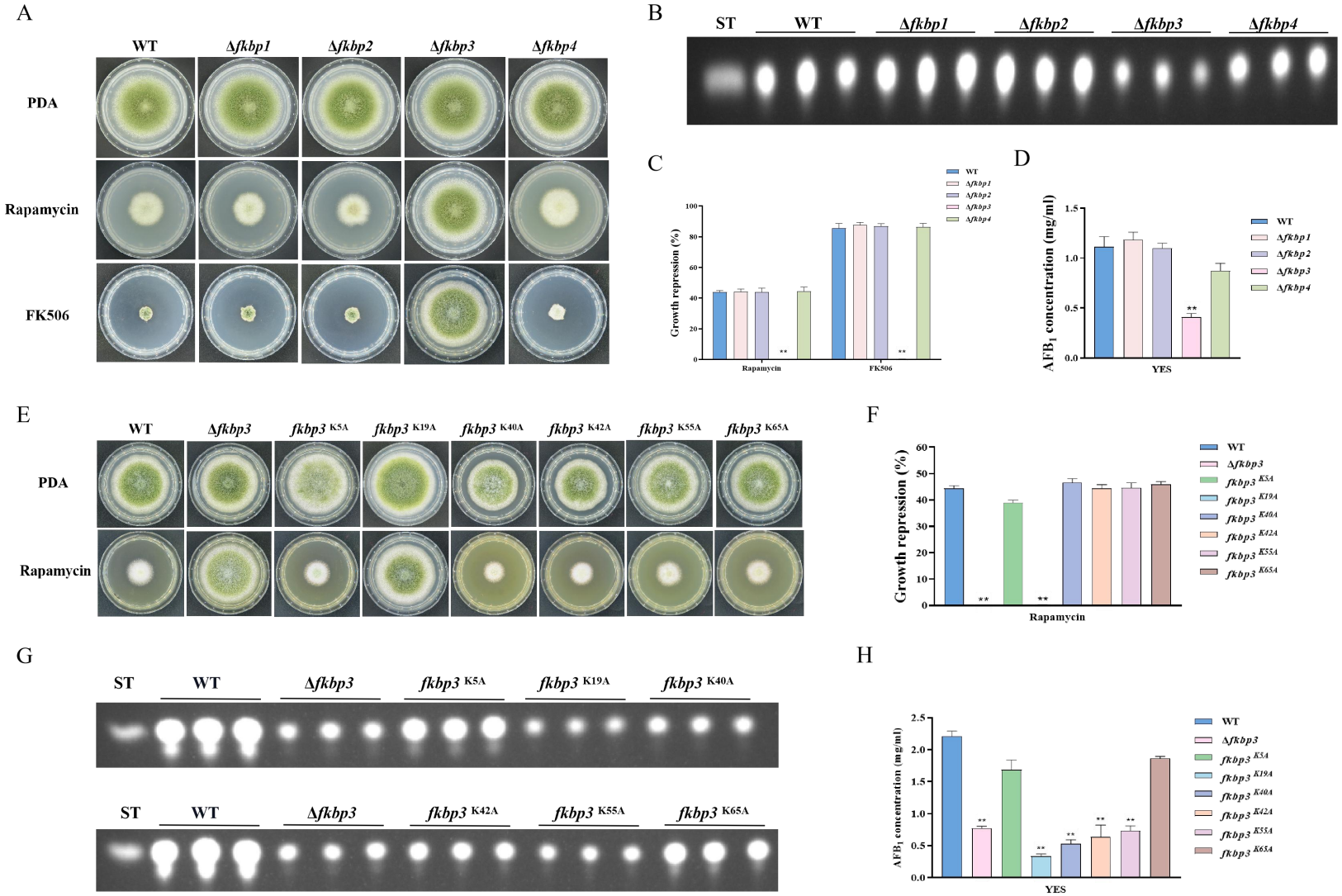
A
WT
Δfkbp1
Δfkbp2
Δfkbp3
Δfkbp4
PDA
Rapamycin
FK506
B
ST
WT
Δfkbp1
Δfkbp2
Δfkbp3
Δfkbp4
C
Growth repression (%)
Rapamycin
FK506
D
AFB1 concentration (mg/ml)
YES
E
WT
Δfkbp3
fkbp3 K5A
fkbp3 K19A
fkbp3 K40A
fkbp3 K42A
fkbp3 K55A
fkbp3 K65A
PDA
Rapamycin
F
Growth repression (%)
Rapamycin
G
ST
WT
Δfkbp3
fkbp3 K5A
fkbp3 K19A
fkbp3 K40A
fkbp3 K42A
fkbp3 K55A
fkbp3 K65A
H
AFB1 concentration (mg/ml)
YES

Fig. 2 Disruption of *fkbp3* significantly increases the resistance of *A. flavus* to rapamycin and FK506.

(A) Phenotype of the WT and all mutant strains (Δ*fkbp1*, Δ*fkbp2*, Δ*fkbp3*, and Δ*fkbp4*) grown on PDA amended with rapamycin and FK506 at 37°C for 5 days.

(B) TLC analysis of AFB_1 production by the WT and all mutant strains (Δ*fkbp1*, Δ*fkbp2*, Δ*fkbp3*, and Δ*fkbp4*) cultured in YES liquid medium at 29°C for 6 days.

(C) The growth inhibition rate of the WT and all mutant strains (Δ*fkbp1*, Δ*fkbp2*, Δ*fkbp3*, and Δ*fkbp4*) under rapamycin and FK506 stress.

(D) AFB_1 quantitative analysis of the WT and all mutant strains (Δ*fkbp1*, Δ*fkbp2*, Δ*fkbp3*, and Δ*fkbp4*) as described in (B).

(E) Phenotype of the WT and all mutant strains (Δ*fkbp3*, K5A, K19A, K40A, K42A, K55A, and K65A) grown on PDA amended with 100 ng/mL rapamycin at 37°C for 5 days.

(F) The growth inhibition rate of the WT and all mutant strains (Δ*fkbp3*, K5A, K19A, K40A, K42A, K55A, and K65A) under rapamycin stress.

(G) TLC assay of AFB_1 production by the WT and all mutant strains (Δ*fkbp3*, K5A, K19A, K40A, K42A, K55A, and K65A) cultured in YES liquid medium at 29°C for 6 days.

(H) Relative quantification of AFB_1 production in the WT and all mutant strains (Δ*fkbp3*, K5A, K19A, K40A, K42A, K55A, and K65A) as mentioned in (G).

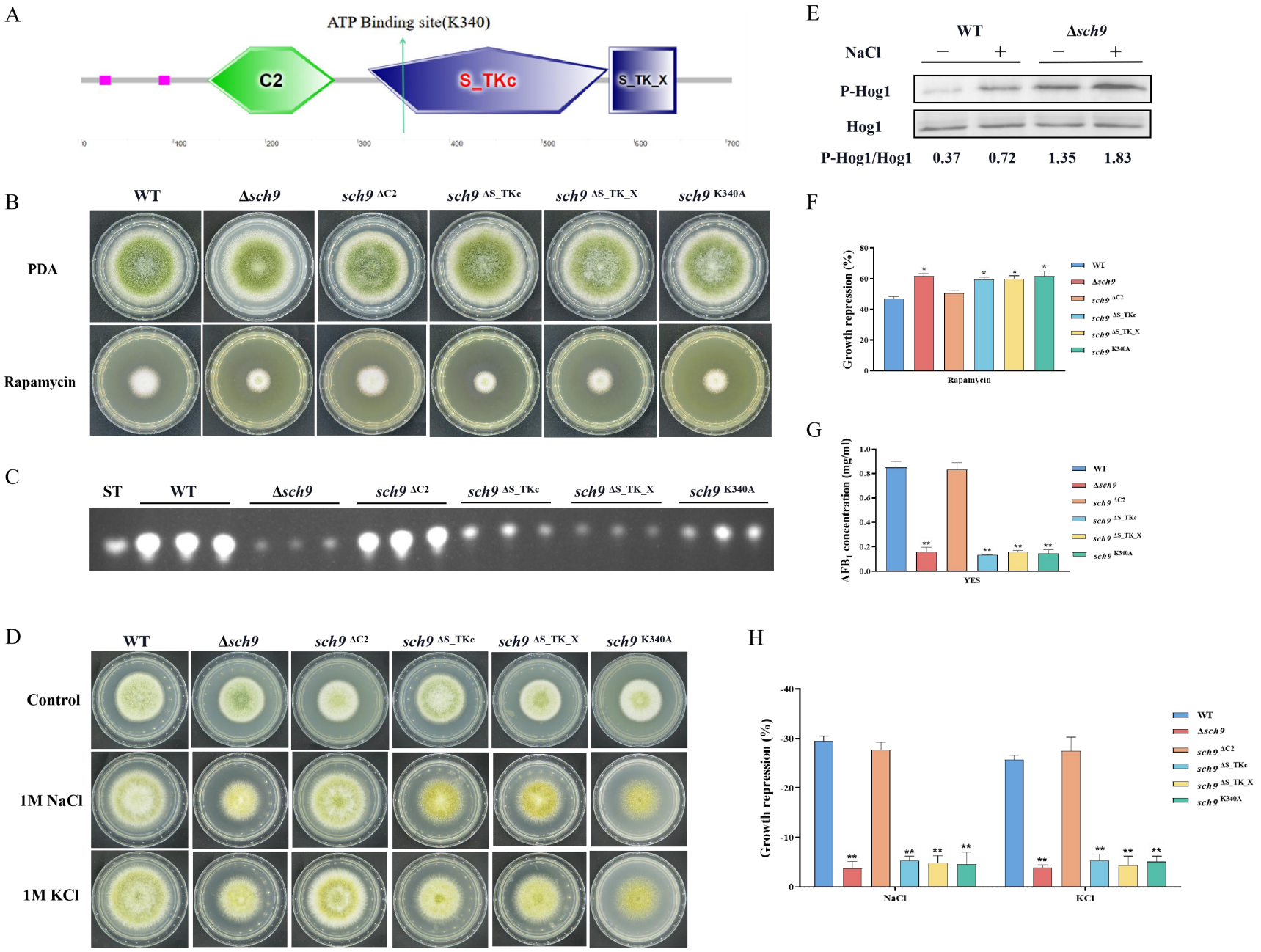
A
ATP Binding site(K340)
C2
S_TKc
S_TK_X
0
100
200
300
400
500
600
700
B
WT
Δsch9
sch9 ΔC2
sch9 ΔS_TKc
sch9 ΔS_TK_X
sch9 K340A
PDA
Rapamycin
C
ST
WT
Δsch9
sch9 ΔC2
sch9 ΔS_TKc
sch9 ΔS_TK_X
sch9 K340A
D
WT
Δsch9
sch9 ΔC2
sch9 ΔS_TKc
sch9 ΔS_TK_X
sch9 K340A
Control
1M NaCl
1M KCl
E
WT
Δsch9
NaCl
−
+
−
+
P-Hog1
Hog1
P-Hog1/Hog1
0.37
0.72
1.35
1.83
F
Growth repression (%)
80
60
40
20
0
Rapamycin
WT
Δsch9
sch9 ΔC2
sch9 ΔS_TKc
sch9 ΔS_TK_X
sch9 K340A
G
AFB1 concentration (mg/ml)
1.0
0.8
0.6
0.4
0.2
0.0
YES
WT
Δsch9
sch9 ΔC2
sch9 ΔS_TKc
sch9 ΔS_TK_X
sch9 K340A
H
Growth repression (%)
-40
-30
-20
-10
0
NaCl
KCl
WT
Δsch9
sch9 ΔC2
sch9 ΔS_TKc
sch9 ΔS_TK_X
sch9 K340A

Fig. 3 The Sch9 kinase participates in aflatoxin biosynthesis and the HOG pathway.

(A) The structure diagram of the Sch9 kinase.

(B) Phenotype of the WT, Δ*sch9*, *sch9*$^{\Delta C2}$, *sch9*$^{\Delta S_TKc}$, *sch9*$^{\Delta S_TK_X}$, and *sch9*^{K340A} strains grown on PDA medium amended with 100 ng/mL rapamycin at 37°C for 5 days.

(C) TLC assay of AFB_1 production from the WT, Δ*sch9*, *sch9*$^{\Delta C2}$, *sch9*$^{\Delta S_TKc}$, *sch9*$^{\Delta S_TK_X}$, and *sch9*^{K340A} strains cultured in YES liquid medium at 29°C for 6 days.

(D) The phenotypes of the WT, Δ*sch9*, *sch9*$^{\Delta C2}$, *sch9*$^{\Delta S_TKc}$, *sch9*$^{\Delta S_TK_X}$, and *sch9*^{K340A}strains on YGT media amended with 1 M NaCl and 1 M KCl for 3 days.

(E) The phosphorylation levels of Hog1 in the WT and Δ*sch9* strains were determined with or without osmotic stress.

(F) The growth inhibition rate of the WT, Δ*sch9*, *sch9*$^{\Delta C2}$, *sch9*$^{\Delta S_TKc}$, *sch9*$^{\Delta S_TK_X}$, and *sch9*^{K340A} strains under rapamycin stress.

(G) Quantitative analysis of AFB_1 as shown in (C).

(H) The growth inhibition rate of the WT, Δ*sch9*, *sch9*$^{\Delta C2}$, *sch9*$^{\Delta S_TKc}$, *sch9*$^{\Delta S_TK_X}$, and *sch9*^{K340A} strains under osmotic stress.

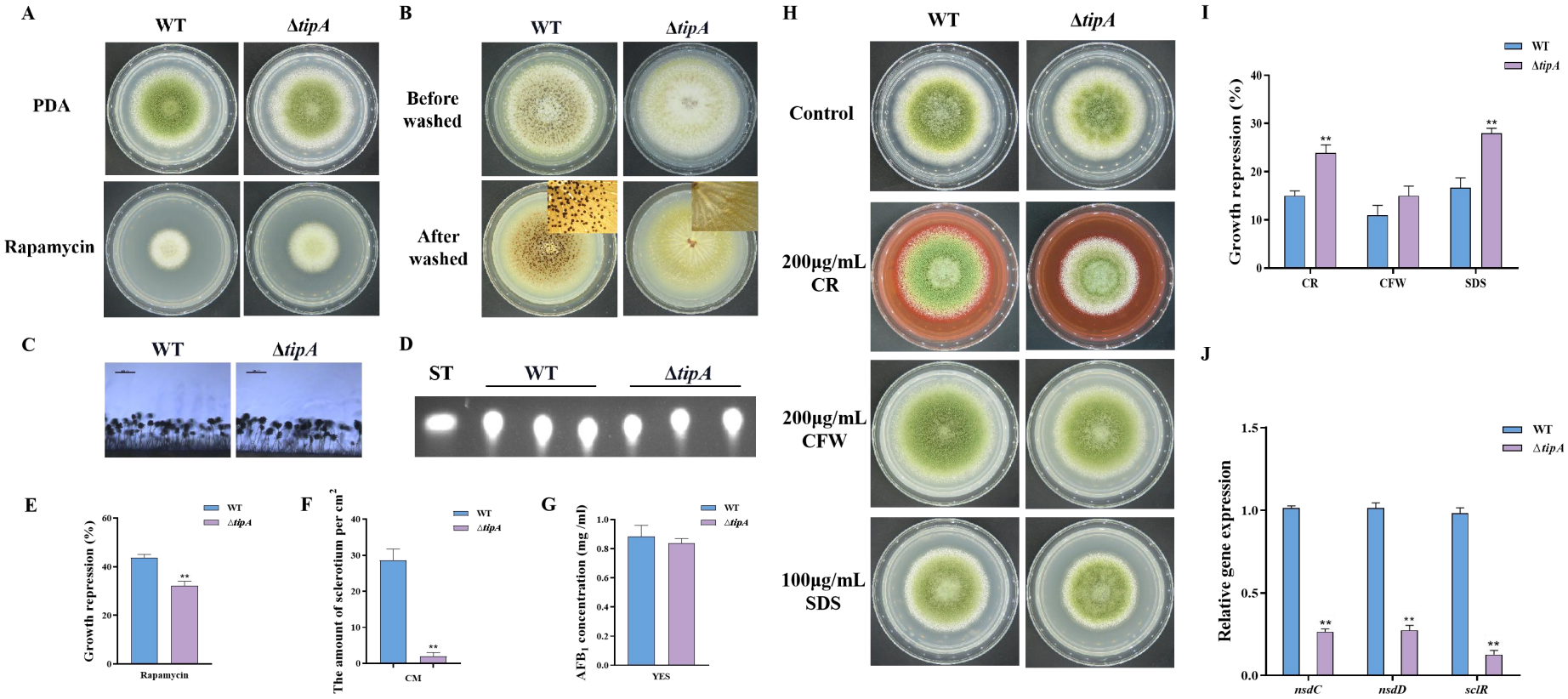
A
WT
ΔtipA
PDA
Rapamycin
B
WT
ΔtipA
Before washed
After washed
H
WT
ΔtipA
Control
200μg/mL CR
200μg/mL CFW
100μg/mL SDS
I
WT
ΔtipA
Growth repression (%)
CR
CFW
SDS
C
WT
ΔtipA
D
ST
WT
ΔtipA
E
WT
ΔtipA
Growth repression (%)
Rapamycin
F
WT
ΔtipA
The amount of sclerotium per cm2
CM
G
WT
ΔtipA
AFB1 concentration (mg /ml)
YES
J
WT
ΔtipA
Relative gene expression
nsdC
nsdD
sclR

Fig. 4 TipA regulates clerotia development and cell wall stress in *A. flavus.*

(A) Phenotype of the WT and Δ*tipA* strains grown on PDA amended with 100 ng/mL rapamycin at 37°C for 5 days.

(B) Phenotypic characterization of the WT and Δ*tipA* strains grown on CM medium at 37°C for 7 days.

(C) Morphology of conidiophores in the WT and Δ*tipA* strains observed by microscope.

(D) TLC assay of AFB_1 production by the WT and Δ*tipA* strains cultured in YES liquid medium at 29°C for 6 days.

(E) The growth inhibition rate of the WT and Δ*tipA* strains under rapamycin stress.

(F) Amount of sclerotia produced by the WT and Δ*tipA* strains.

(G) AFB_1 quantitative analysis of the WT and Δ*tipA* strains described in (D).

(H) Colony morphology of the WT and Δ*tipA* strains grown on PDA media supplemented with 200 μg/mL CR, 200μg/mL CFW, and 100 μg/mLSDS at 37°C for 5 days.

(I) The growth inhibition rate of the WT and Δ*tipA* strains under cell wall and cell membrane stress.

(J) Relative expression levels of sclerotia formation genes in the WT and Δ*tipA* strains.

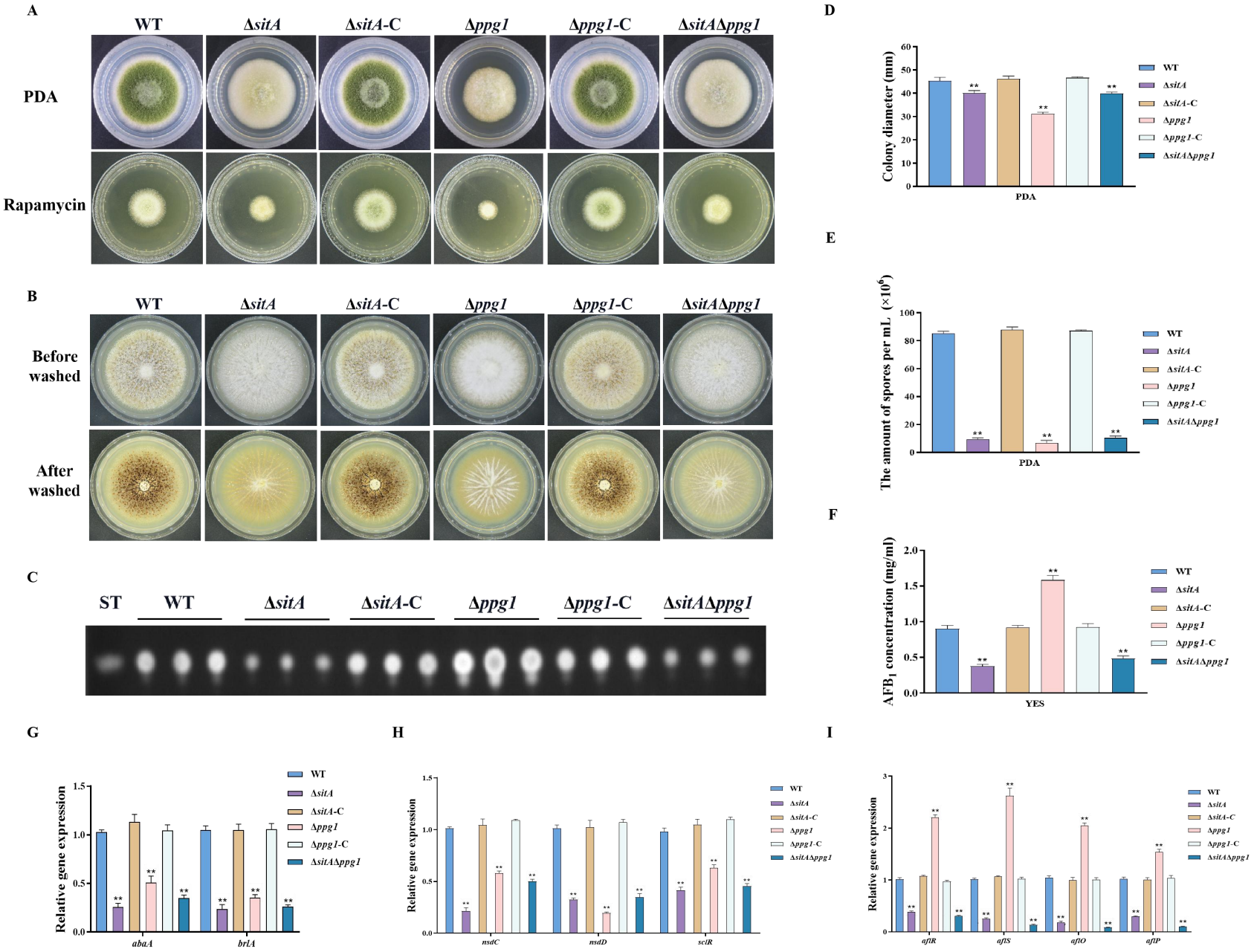
A
WT
ΔsitA
ΔsitA-C
Δppg1
Δppg1-C
ΔsitAΔppg1
PDA
Rapamycin
B
Before washed
After washed
C
ST
D
Colony diameter (mm)
PDA
E
The amount of spores per mL (×10^6)
F
AFB1 concentration (mg/ml)
YES
G
Relative gene expression
abaA
brlA
H
nsdC
nsdD
sclR
I
aflR
aflS
aflO
aflP

Fig. 5 The impact of the phosphatases SitA and Ppg1 on the growth, conidiation, and aflatoxin biosynthesis in *A. flavus*.

(A) Colony morphology of the WT, single knockout, and double knockout strains cultured on PDA medium amended with 100 ng/mL rapamycin at 37℃ for 5 days.

(B) Colony morphology of the WT, single knockout, and double knockout strains cultured on CM medium at 37℃ for 7 days.

(C) TLC analysis of AFB_1 production from the WT, single knockout, and double knockout strains cultured in YES liquid medium at 29℃ for 6 days.

(D) Growth diameter of the WT, single knockout, and double knockout strains on PDA media.

(E) The growth inhibition rate of the WT, single knockout, and double knockout strains under rapamycin stress.

(F) AFB_1 quantitative analysis of the WT, single knockout, and double knockout strains.

(G) Relative expression levels of conidia synthesis genes in the WT, single knockout, and double knockout strains.

(H) Relative expression levels of sclerotia synthesis genes in the WT, single knockout, and double knockout strains.

(I) Relative expression levels of aflatoxin biosynthesis genes in the WT, single knockout, and double knockout strains.

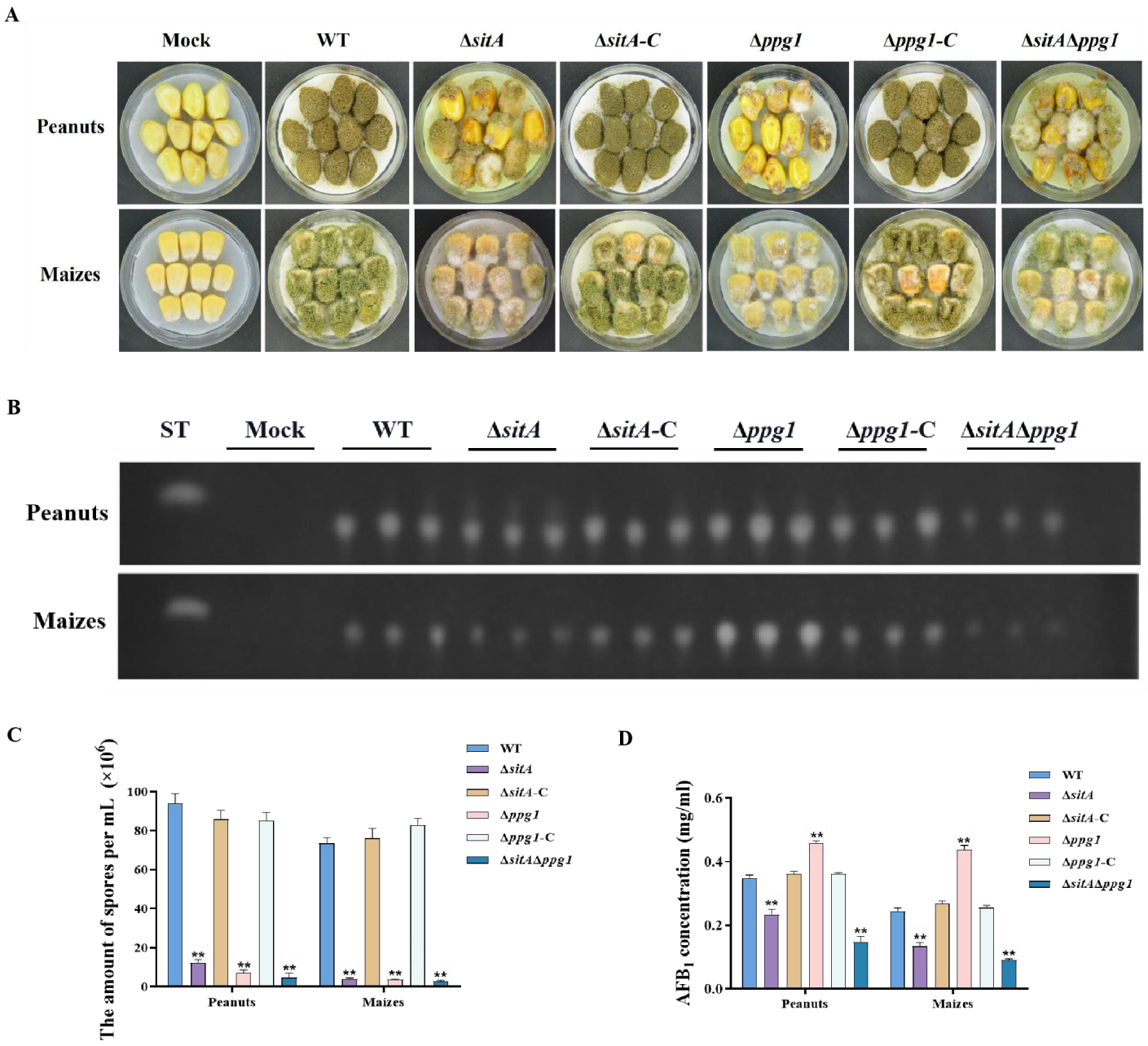
A
Mock
WT
ΔsitA
ΔsitA-C
Δppg1
Δppg1-C
ΔsitAΔppg1
Peanuts
Maizes
B
ST
Mock
WT
ΔsitA
ΔsitA-C
Δppg1
Δppg1-C
ΔsitAΔppg1
Peanuts
Maizes
C
The amount of spores per mL (×10^6)
100
80
60
40
20
0
Peanuts
Maizes
WT
ΔsitA
ΔsitA-C
Δppg1
Δppg1-C
ΔsitAΔppg1
D
AFB1 concentration (mg/ml)
0.6
0.4
0.2
0.0
Peanuts
Maizes
WT
ΔsitA
ΔsitA-C
Δppg1
Δppg1-C
ΔsitAΔppg1

Fig. 6 Pathogenicity analysis of the phosphatase SitA and Ppg1 in *A. flavus*.

(A) Phenotypes of peanut and maize infected by the WT, single knockout, and double knockout strains.

(B) TLC was used to detect the AFB_1 from peanut and maize infected by the WT, single knockout, and double knockout strains.

(C) Quantitative analysis of conidia production from peanut and maize infected by the WT, single knockout, and double knockout strains.

(D) Quantitative analysis of AFB_1 from peanut and maize infected by the WT, single knockout, and double knockout strains.

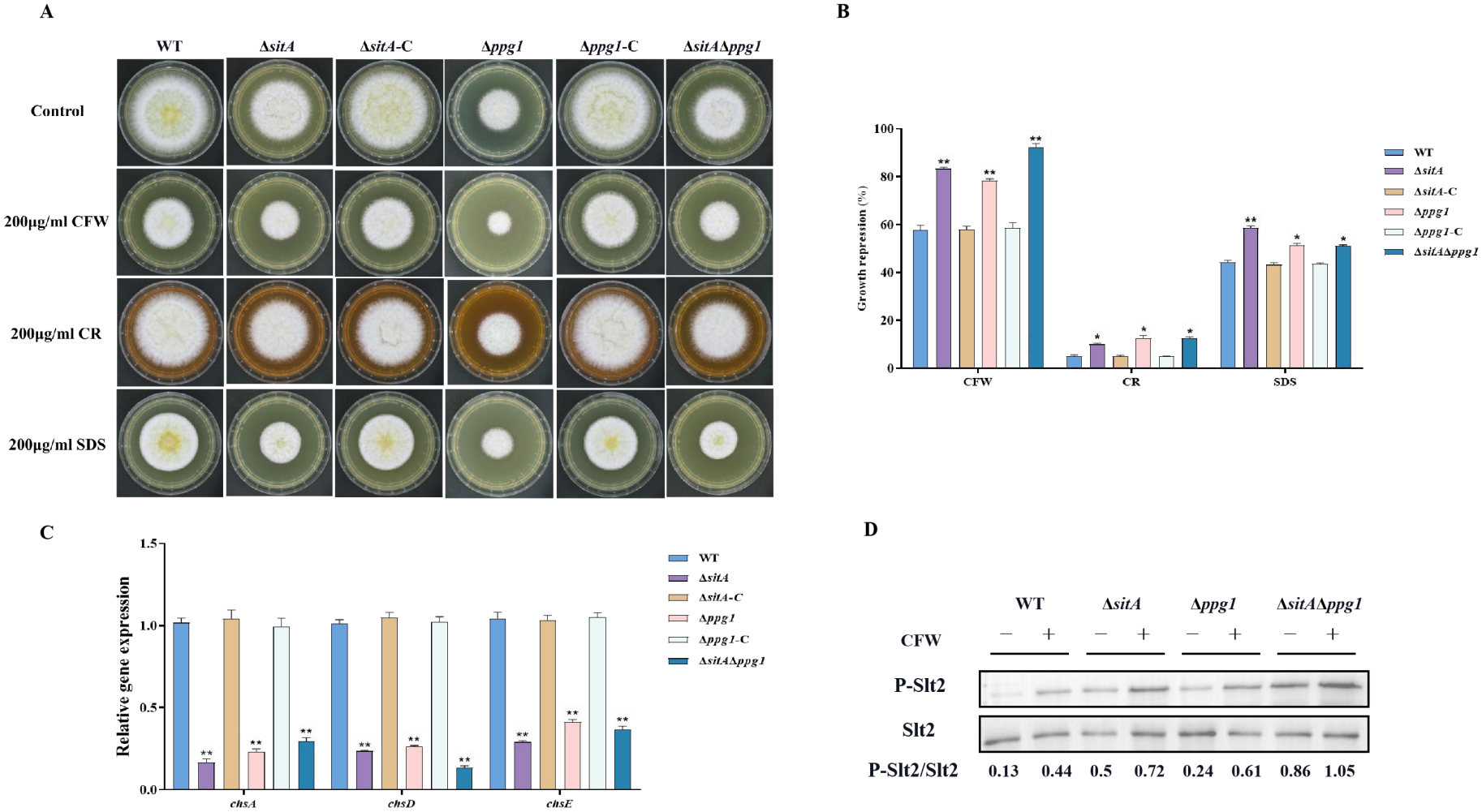
A
WT
ΔsitA
ΔsitA-C
Δppg1
Δppg1-C
ΔsitAΔppg1
Control
200μg/ml CFW
200μg/ml CR
200μg/ml SDS
B
Growth repression (%)
100
80
60
40
20
0
CFW
CR
SDS
WT
ΔsitA
ΔsitA-C
Δppg1
Δppg1-C
ΔsitAΔppg1
C
Relative gene expression
1.5
1.0
0.5
0.0
chsA
chsD
chsE
WT
ΔsitA
ΔsitA-C
Δppg1
Δppg1-C
ΔsitAΔppg1
D
WT
ΔsitA
Δppg1
ΔsitAΔppg1
CFW
− + − + − + − +
P-Slt2
Slt2
P-Slt2/Slt2
0.13 0.44 0.5 0.72 0.24 0.61 0.86 1.05

Fig. 7 Sensitivity of phosphatase SitA and Ppg1 to cell wall damaging agents in *A. flavus*.

(A) Morphology of the WT, single knockout, and double knockout strains grown on YES media supplemented with 200 μg/mL CR, 200 μg/mL CFW, or 100 μg/mL SDS at 37°C for 5 days.

(B) The growth inhibition rate of the WT, single knockout, and double knockout strains under cell wall and cell membrane stress.

(C) Relative expression levels of cell wall synthesis genes (*chsA*, *chsD* and *chsE*) in the WT, single knockout, and double knockout strains.

(D) The phosphorylation level of Slt2 in the WT, single knockout, and double knockout strains was detected with or without cell wall stress.

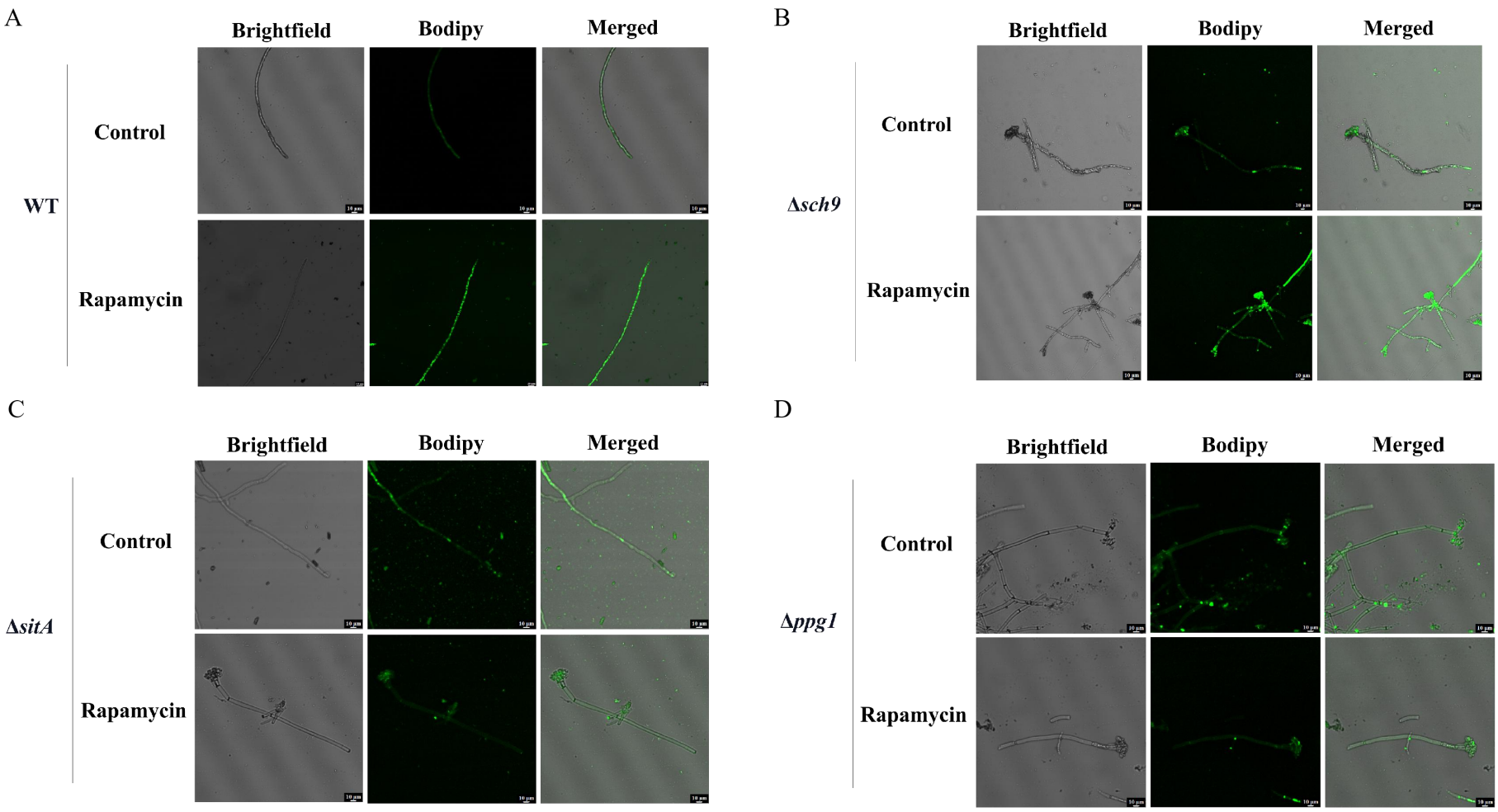
A
Brightfield
Bodipy
Merged
WT
Control
Rapamycin
B
Brightfield
Bodipy
Merged
Δsch9
Control
Rapamycin
C
Brightfield
Bodipy
Merged
ΔsitA
Control
Rapamycin
D
Brightfield
Bodipy
Merged
Δppg1
Control
Rapamycin

Fig. 8 Phosphatase SitA and Ppg1 are involved in regulating lipid droplet biogenesis.

(A) The intracellular lipid droplets were stained by boron dipyrromethene difluoride (BODIPY) in hyphae of the WT strain and observed under fluorescence microscopy. The phenotype of lipid droplets accumulation in the mycelia of the WT strain treated with or without 100 ng/mL rapamycin for 6 h (Bar, 10 μm).

(B) Phenotype of lipid droplets accumulation in the mycelia of the Δ*sch9* strain treated with or without 100 ng/mL rapamycin for 6 h (Bar, 10 μm).

(C) Phenotype of lipid droplets accumulation in the mycelia of the Δ*sitA* strain treated with or without 100 ng/mL rapamycin for 6 h (Bar, 10 μm).

(D) Phenotype of lipid droplets accumulation in the mycelia of the Δ*ppg1* strain treated with or without 100 ng/mL rapamycin for 6 h (Bar, 10 μm).

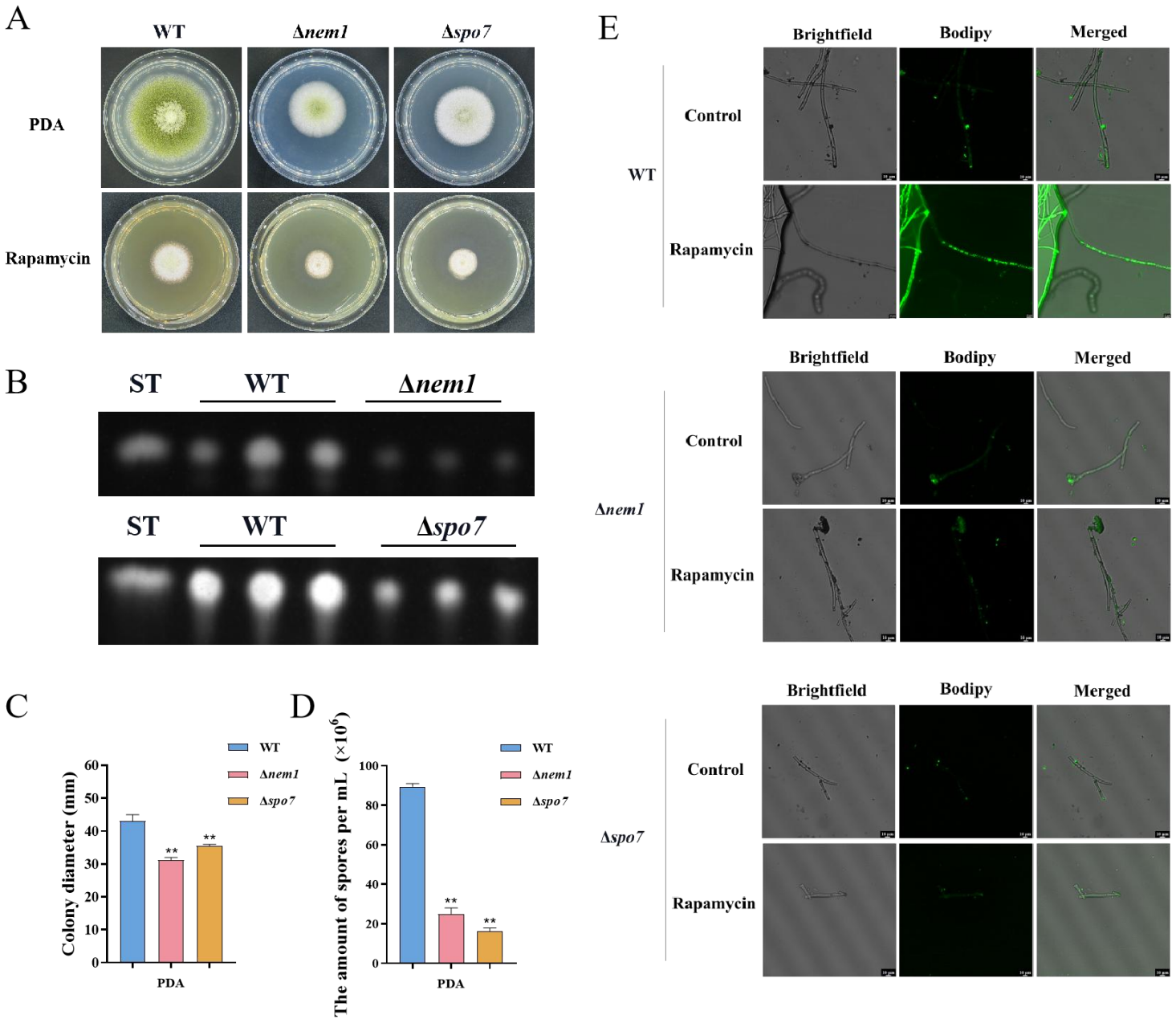
A
WT
Δnem1
Δspo7
PDA
Rapamycin
B
ST
WT
Δnem1
ST
WT
Δspo7
C
Colony diameter (mm)
WT
Δnem1
Δspo7
PDA
D
The amount of spores per mL (×10^6)
WT
Δnem1
Δspo7
PDA
E
Brightfield
Bodipy
Merged
WT
Control
Rapamycin
Δnem1
Control
Rapamycin
Δspo7
Control
Rapamycin

Fig. 9 Phosphatase complex Nem1/Spo7 play significant role in growth, conidiation, aflatoxin, and lipid droplet biogenesis.

(A) Phenotype of the WT, Δ*nem1*, and Δ*spo7* strains grown on PDA amended with 100 ng/mL rapamycin at 37°C for 5 days.

(B) TLC assay of AFB_1 production from the WT, Δ*nem1*, and Δ*spo7* strains cultured in YES liquid medium at 29°C for 6 days.

(C) Growth diameter of the WT, Δ*nem1*, and Δ*spo7* strains on PDA media.

(D) Statistical analysis of the sporulation by the WT, Δ*nem1*, and Δ*spo7* strains.

(E) Phenotype of lipid droplets accumulation in the mycelia of the WT, Δ*nem1*, and Δ*spo7* strains treated with or without 100 ng/mL rapamycin for 6 h (Bar, 10 μm).

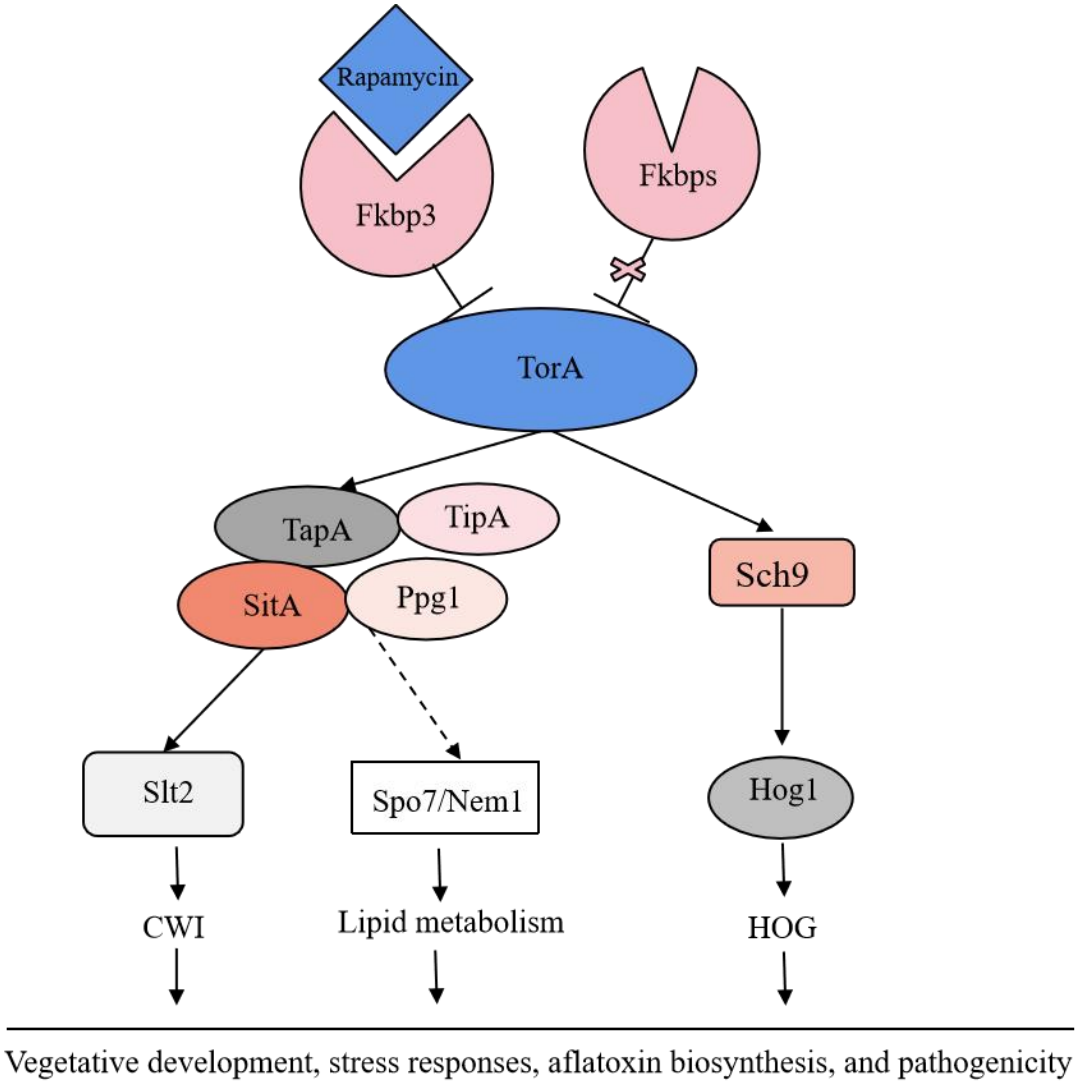
Rapamycin
Fkbp3
Fkbps
TorA
TapA
TipA
SitA
Ppg1
Sch9
Slt2
Spo7/Nem1
Hog1
CWI
Lipid metabolism
HOG
Vegetative development, stress responses, aflatoxin biosynthesis, and pathogenicity

Fig. 10 The proposed model of the target of rapamycin (TOR) pathway in *A. flavus*.

Based on the above results, we propose a hypothesis regarding the TOR signaling pathway model in *A. flavus.* Rapamycin forms a complex with Fkbp3, and this particular complex can bind to the TorA kinase, thereby impeding its regular functionality. Sch9, functioning as a downstream element of the TorA kinase, regulates aflatoxin biosynthesis and HOG signaling pathway. As another important target of the TorA kinase, TapA-phosphatase complex is involved in the regulation of growth, sporulation, sclerotia, aflatoxin production, CWI signaling pathway, lipid droplet synthesis, and other processes. In conclusion, the TOR signaling pathway plays a crucial role in various aspects of *A. flavus*, including vegetative development, stress response, aflatoxin biosynthesis, and pathogenicity.